Accepted to the Astrophysical Journal: Feb 5, 2002
Preprint typeset using LaTeX style emulateapj v. 14/09/00

THE UCSD HIRES/KECK I DAMPED Lyα ABUNDANCE DATABASE[1] III. AN EMPIRICAL STUDY OF PHOTOIONIZATION IN THE DAMPED Lyα SYSTEM TOWARD GB1759+7539

JASON X. PROCHASKA[2,3]
The Observatories of the Carnegie Institute of Washington
813 Santa Barbara St. Pasadena, CA 91101
xavier@ociw.edu

AND

J. CHRISTOPHER HOWK
Department of Physics and Astronomy; Johns Hopkins University;
3400 North Charles St.; Baltimore, MD 21218
howk@pha.jhu.edu

AND

JOHN M. O'MEARA[2], DAVID TYTLER[2], ARTHUR M. WOLFE[2], DAVID KIRKMAN[2],
DAN LUBIN, & NAO SUZUKI
Department of Physics, and Center for Astrophysics and Space Sciences
University of California, San Diego; C–0424; La Jolla, CA 92093
jomeara@ucsd.edu, dtytler@ucsd.edu, awolfe@ucsd.edu, dkirkman@ucsd.edu dlubin@ucsd.edu, n1suzuki@ucsd.edu
Accepted to the Astrophysical Journal: Feb 5, 2002

ABSTRACT

We investigate the ionization state of the damped Lyα system at $z = 2.62$ toward GB1759+7539 through an analysis of ionic ratios sensitive to photoionization: $\mathrm{Ar^0/S^+}$, $\mathrm{Fe^{++}/Fe^+}$, $\mathrm{N^+/N^0}$, $\mathrm{Al^{++}/Al^+}$. Approximately half of the metals arise in a mostly neutral velocity component with $\mathrm{H\,I/H} > 0.9$, based on $\mathrm{Fe^{++}/Fe^+} < 0.013$. In contrast, the remaining half exhibits $\mathrm{Fe^{++}/Fe^+} \approx 0.3$ indicative of a partially ionized medium with $\mathrm{H\,I/H} \approx 0.5$. These conclusions are supported by the observed $\mathrm{N^+/N^0}$, $\mathrm{Al^{++}/Al^+}$, and $\mathrm{Ar^0/Si^+}$ ratios.

We assess ionization corrections for the observed column densities through photoionization models derived from the CLOUDY software package. In the neutral gas, the ionization corrections are negligible except for $\mathrm{Ar^0}$. However for the partially ionized gas, element abundance ratios differ from the ionic ratios by 0.1 – 0.3 dex for ($\mathrm{Si^+}$, $\mathrm{S^+}$, $\mathrm{Ni^+}$, $\mathrm{Al^+}$)/$\mathrm{Fe^+}$ ratios and more for ($\mathrm{N^0}$, $\mathrm{Ar^0}$)/$\mathrm{Fe^+}$. Independent of the shape of the photoionizing spectrum and assumptions on the number of ionization phases, these ionization corrections have minimal impact ($\lesssim 0.1$ dex) on the total metallicity inferred for this damped Lyα system. Measurements on the relative elemental abundances of the partially ionized gas, however, have a greater than $\approx$0.15 dex uncertainty which hides the effects of nucleosynthesis and dust depletion.

We caution the reader that this damped system is unusual for a number of reasons (e.g. a very low $\mathrm{Ar^0/S^+}$ ratio) and we believe its ionization properties are special but not unique. Nevertheless, it clearly shows the value of examining photoionization diagnostics like $\mathrm{Fe^{++}/Fe^+}$ in a larger sample of systems.

Subject headings: galaxies: abundances — galaxies: chemical evolution — quasars : absorption lines — nucleosynthesis

1. INTRODUCTION

Through echelle optical spectroscopy of the damped Lyα systems – quasar absorption line systems with $N(\mathrm{HI}) \geq 2 \times 10^{20}\,\mathrm{cm^{-2}}$ – one studies the chemical abundances of high redshift galaxies in a manner analogous with UV spectroscopy of the Galactic ISM. These observations yield ionic column density measurements of a series low-ions[4] including $\mathrm{Si^+}$, $\mathrm{Fe^+}$, $\mathrm{Ni^+}$, $\mathrm{Zn^+}$, $\mathrm{S^+}$, and $\mathrm{N^0}$ (e.g. Lu et al. 1996; Prochaska & Wolfe 1999; Molaro et al. 2000; Prochaska et al. 2001), often at a greater accuracy than measurements of the Galactic ISM. By studying these chemical abundances, one gains insight into the nucleosynthetic enrichment, dust properties, and metallicity of the damped Lyα systems and thereby the high redshift protogalactic population (e.g. Prochaska & Wolfe 2002).

To date, most damped Lyα abundance studies have proceeded under the assumption that the gas has a very low ionization fraction,

$$x \equiv \frac{\mathrm{H^+}}{\mathrm{H^0} + \mathrm{H^+}} \ll 1 \quad . \tag{1}$$

In this case, the low-ion species represent the dominant ionization states and ionization corrections for elemental abundances are small, e.g. $N(\mathrm{Si}) \simeq N(\mathrm{Si^+})$. There is a good theoretical basis for adopting this assumption. Prochaska & Wolfe (1996) performed a series of radiative transfer calculations and predicted $x < 10\%$ for systems with $N(\mathrm{HI}) > 10^{20}\,\mathrm{cm^{-2}}$. Furthermore, the authors compared observed $\mathrm{Al^{++}/Al^+}$ and $\mathrm{Si^{3+}/Si^+}$ ratios for the damped Lyα systems against a series of photoionization models derived from the CLOUDY software package (v. 95; Ferland 2001) and concluded it has an ionization frac-

[1] http://kingpin.ucsd.edu/~hiresdla

[2] Visiting Astronomer, W.M. Keck Telescope. The Keck Observatory is a joint facility of the University of California and the California Institute of Technology.

[3] Hubble fellow

[4] The term low-ion refers to the dominant ionic state of a given element in an HI region.

tion $x < 50\%$. Viegas (1995) reached similar conclusions for systems with $N(\mathrm{HI}) > 10^{21}\,\mathrm{cm}^{-2}$ but warned that ionization corrections could be important in systems with $N(\mathrm{HI}) \approx 10^{20}\,\mathrm{cm}^{-2}$. More recently, Howk & Sembach (1999) argued that photoionization could imply significant corrections for some ionic species in the damped Lyα systems, particularly if there were a significant local source of ionization (e.g. recent star formation). Vladilo et al. (2001) have extended this analysis further and concluded that ionization corrections are a concern for only a few of the elements (e.g. Al) observed in the damped systems. Finally, Izotov, Schaerer, & Charbonnel (2001) have presented a specific model for the damped Lyα systems which suggests large ionization corrections for a number of elements. This model predicts $\mathrm{O}^0/\mathrm{Si}^+$ ratios, however, which are much lower than those typically observed in the damped Lyα systems.

All of these studies have presented theoretical arguments which require idealized physical conditions (e.g. constant volume density, plane-parallel geometry), unknown quantities (e.g. shape, flux of the ionizing radiation), and uncertain physics (e.g. dielectric recombination rates). To overcome many of these uncertainties, one can empirically determine the ionization state of the gas by measuring adjacent ions of several elements (e.g. $\mathrm{Fe}^{++}/\mathrm{Fe}^+$). Observationally, this requires an analysis of transitions like Si III $\lambda1206$, Fe III $\lambda1122$, and N II $\lambda1083$ all of which arise in the Lyα forest and typically at observed wavelength $\lambda < 4000$Å. Unfortunately, we have not tended to acquire these observations because of the limited wavelength coverage of the HIRES spectrograph in one setting and its poor sensitivity below 4000 Å. Therefore, the large damped Lyα databases provided by the Keck community (Lu et al. 1996; Prochaska & Wolfe 1999; Pettini et al. 1999; Prochaska et al. 2001) have not directly addressed ionization corrections for the damped Lyα abundances. Similarly, other studies in the literature (e.g. Fan & Tytler 1994) have only focused on ratios like $\mathrm{C}^{3+}/\mathrm{C}^+$ which provide a less precise evaluation of photoionization.

In this paper, we examine the photoionization of a single damped Lyα system through observations of a series of ions sensitive to the ionization state of the gas. We present a case study of the $z_{abs} = 2.62$ damped Lyα system toward GB1759+7539 ($z_{em} = 3.05$, V≈17). This sightline has been previously analysed by Prochaska & Wolfe (1999), Outram, Chaffee, & Carswell (1999), and Prochaska et al. (2001), but none of these studies focused on the ionization state of the damped Lyα system. Here, we present observations of a series of metal-line transitions which indicate this damped Lyα system is partially ionized. Before proceeding, we emphasize that this damped Lyα system was selected on the basis that it exhibits several transitions suggestive of photoionization (e.g. strong Si III 1206 absorption). Therefore, *the system may not be representative of the damped Lyα population.* In fact, there are at least four peculiar characteristics of this damped system:

1. It is the only known damped system with a significantly sub-solar $\mathrm{Ar}^0/\mathrm{Si}^+$ ratio (Prochaska & Wolfe 2002).

2. It is one of the few systems where the low-ions do not uniformly track one another in velocity space.

3. It is one of the few systems where the Al III profile shows significant departures from the low-ion profiles (Wolfe & Prochaska 2000).

4. It is one of the few systems where the C II* profile does not closely trace the low-ion profiles (Wolfe, Prochaska, & Gawiser 2002).

Interestingly, these characteristics are in much better general agreement with gas probed in the Galactic ISM than with other damped systems (e.g. Savage and Sembach 1996). Irrespective of the peculiar nature of the damped system toward GB1759+7539, our analysis emphasizes the importance of observations of Si III, Fe III, N II, Ar I and other transitions for assessing the impact of photoionization on the chemical abundances one derives from low-ion transitions.

Table 1
ATOMIC DATA

Transition	λ	f	Ref
SiIII 1012	1012.5020	0.03550000	1
ArI 1048	1048.2199	0.26280000	3
ArI 1066	1066.6600	0.06747000	3
NII 1083	1083.9900	0.10310000	1
FeIII 1122	1122.5260	0.16200000	3
NI 1134a	1134.1653	0.01342000	1
NI 1134b	1134.4149	0.02683000	1
NI 1134c	1134.9803	0.04023000	1
FeII 1143	1143.2260	0.01770000	2
SiII 1193	1193.2897	0.49910000	1
NI 1199	1199.5496	0.13280000	1
NI 1200a	1200.2233	0.08849000	1
NI 1200b	1200.7098	0.04423000	1
SiIII 1206	1206.5000	1.66000000	1
SII 1250	1250.5840	0.00545300	1
CII 1334	1334.5323	0.12780000	1
CII* 1335	1335.7077	0.11490000	1
NiII 1370	1370.1310	0.07690000	5
SiIV 1393	1393.7550	0.52800000	1
SiIV 1402	1402.7700	0.26200000	1
SiII 1526	1526.7066	0.12700000	9
CIV 1548	1548.1950	0.19080000	1
CIV 1550	1550.7700	0.09522000	1
FeII 1608	1608.4511	0.05800000	17
FeII 1611	1611.2005	0.00136000	16
AlII 1670	1670.7874	1.88000000	1
NiII 1709	1709.6042	0.03240000	7
NiII 1741	1741.5531	0.04270000	7
SiII 1808	1808.0130	0.00218000	11
AlIII 1854	1854.7164	0.53900000	1
ZnII 2026	2026.1360	0.48900000	13
CrII 2066	2066.1610	0.05150000	13

References. — Key to References – 1: Morton (1991); 2: Howk et al. (2000); 3: Morton (2002); 5: Fedchak & Lawler (1999); 7: Fedchak, Wiese, & Lawler (2000); 9: Schectman, Povolny, & Curtis (1998); 10: Bergeson et al. (1996); 11: Bergeson & Lawler (1993); 13: Bergeson & Lawler (1993b); 17: Bergeson, Mullman, & Lawler (1996b)

Note. — See http://kingpin.ucsd.edu/∼hiresdla for the most current and complete version of this table.

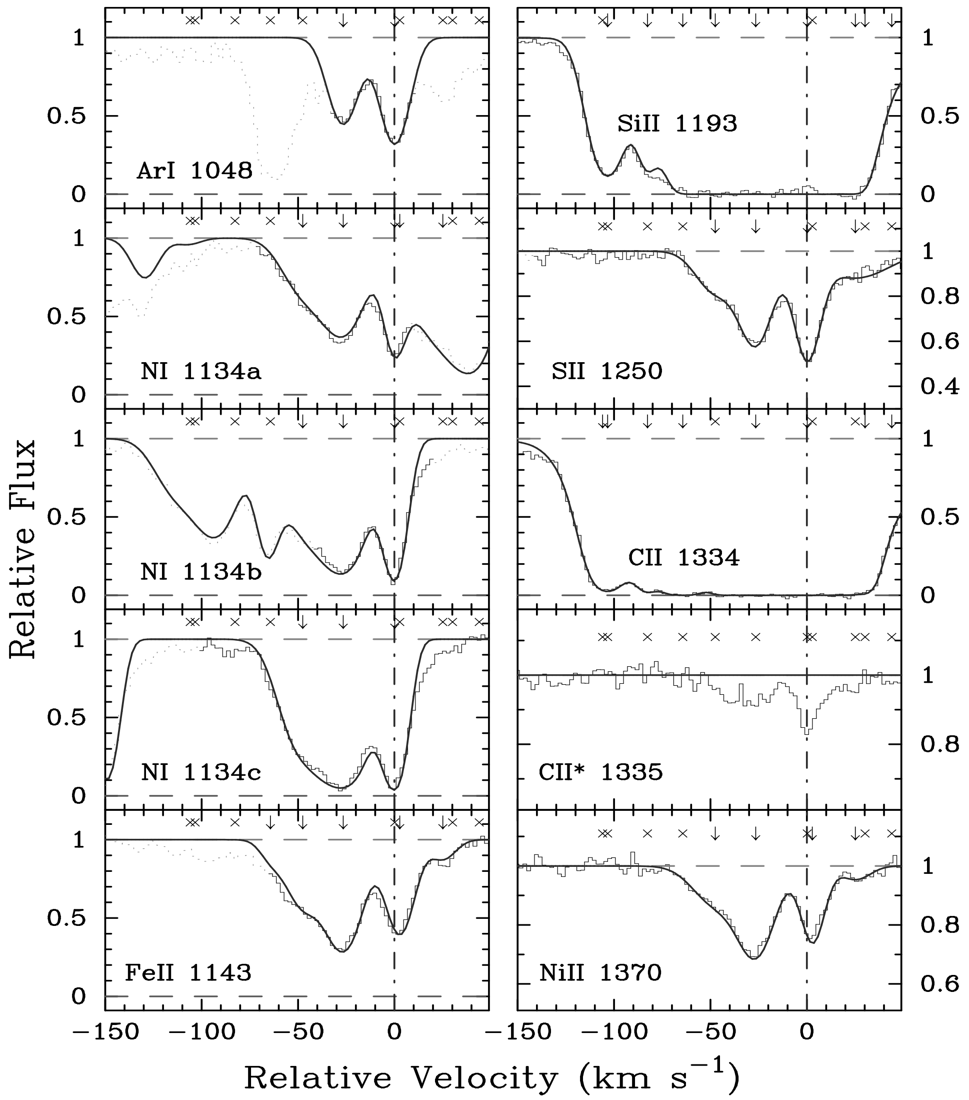

FIG. 1.— Velocity profiles of low-ion transitions from the $z_{abs} = 2.62$ damped Lyα system toward GB1759+7539. In the figure, $v = 0$ km/s corresponds to $z = 2.62561$. Most of the transitions are overplotted with a profile fit derived with the VPFIT software package. The marks (arrows and x's) at the top of each panel indicate all of the velocity components included in the fits. The arrows designate the components included in the analysis of a specific ion whereas the x's have been excluded. Known blends have been dotted out in the figure.

2. IONIC COLUMN DENSITIES

The quasar GB1759+7539 has been observed by at least three groups (Prochaska & Wolfe 1999; Outram, Chaffee, & Carswell 1999; Prochaska et al. 2001) with the HIRES spectrograph (Vogt et al. 1994) on the Keck I telescope. We have combined these data to produce a spectrum with nearly continuous wavelength coverage from $\lambda = 3400 - 7590$Å. The Prochaska & Wolfe (1999) and Prochaska et al. (2001) data sets were combined without coadding because the spectral coverage did not overlap. Therefore, the resolution of the original observations was preserved at 6 km/s and 8 km/s respectively. Finally, we included the data Outram, Chaffee, & Carswell (1999) to fill in the inter-order gaps longward of ≈ 5000 Å. In terms of the damped Lyα system at $z = 2.625$ ($\log N$(HI) $= 20.761 \pm 0.007$; Outram et al. 1999), the observations present measurements of transitions ranging from S III 1012 to Cr II 2066.

In the following sub-sections we derive ionic column densities for the majority of transitions identified for this damped system. We have performed a line-profile fitting analysis using the VPFIT software package[5] kindly provided by R. Carswell and J. Webb. This least-squares routine minimizes a χ^2 matrix of multiple component Voigt profile fits to observed line profiles. Each velocity component is described by three parameters – column density, redshift, and Doppler parameter (b-value) – which can selectively be 'tied' together from ion to ion. It should be noted that line blending can lead to significant uncertainties in the Doppler parameter and sometimes redshift of various components. On the other hand, our experience

[5] http://www.ast.cam.ac.uk/~rfc/vpfit.html

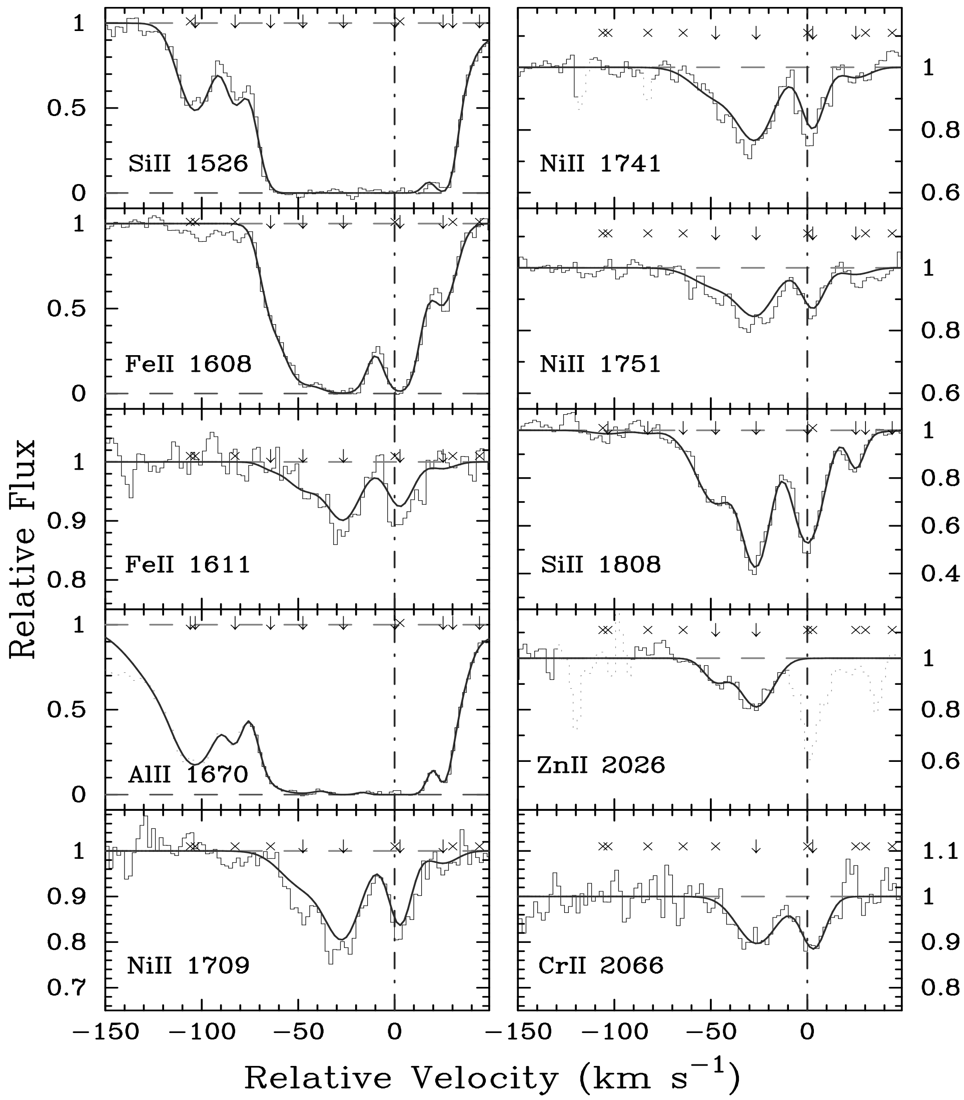

Fig1 – cont

is that the column densities remain reasonably robust for unsaturated profiles. It is important to note that we include solutions for a number of heavily saturated profiles. These components are easily identified by their very large reported uncertainties and they have not been included in the analysis. Furthermore, some velocity components have large uncertainties because of a degeneracy in the solution (e.g. two velocity components which nearly overlap). We have taken care to insure that these line blending effects have not influenced our photoionization analysis. Finally, Table 1 presents the atomic data used for the metal-line transitions analysed in this paper.

2.1. *Low-Ion Profiles*

Figure 1 presents velocity profiles for the most important low-ion transitions in our analysis. The velocity profiles are comprised of two main features at $v \approx 0$ and -25 km/s where $v = 0$ km/s corresponds to the redshift $z = 2.62561$. Contrary to the majority of damped Lyα systems, it is obvious from the figure that the relative abundances of these two components are not constant from ion to ion. The differences are less severe than the visual impression, but are greater than 0.1 dex (i.e. $> 3\sigma$) in several cases. This is a rare occurrence in the damped Lyα systems (see Prochaska et al. 2001) and it raises the likelihood that this system is peculiar.

Table 2 presents the full VPFIT solution and errors for the low-ion profiles derived with the VPFIT software package. In Figure 1, most of the transitions are overplotted with the profile fit and the marks (arrows and x's) at the top of each panel indicate all of the velocity components included in the fits. The arrows designate the components included in the analysis of a specific ion whereas the x's identify excluded components. In general, all of the low-ions were fit with 3–7 components with tied redshifts. In contrast to our previous experience with VPFIT solutions

TABLE 2
IONIC COLUMN DENSITIES: LOW-IONS

ID	z_{abs}	$\sigma(z)$ (10^{-5})	v_{rel}[a] (km/s)	Ion	$\log N$ (cm^{-2})	$\sigma(N)$	b (km/s)	$\sigma(b)$
1	2.624329	4.1	−105	C^+	13.747	0.514	20.41	12.68
				Al^+	12.677	0.093	29.23	5.28
2	2.624360	0.3	−103	Si^+	13.452	0.010	10.67	0.32
				C^+	14.160	0.237	11.24	2.78
				Al^+	12.428	0.164	11.48	1.65
3	2.624610	0.4	−82	Si^+	13.164	0.042	5.84	0.65
				C^+	14.042	0.082	6.37	1.68
				Al^+	12.008	0.093	4.94	0.77
4	2.624832	1.3	−64	Si^+	13.505	0.365	8.76	1.55
				Fe^+	13.453	0.136	6.32	1.04
				C^+	14.794	1.180	7.21	5.14
				Al^+	12.383	0.409	7.77	1.82
5	2.625035	0.8	−47	Si^+	14.902	0.050	12.40	1.69
				Fe^+	14.331	0.039	11.03	1.12
				N^0	14.401	0.038	13.72	1.19
				Al^+	13.196	0.119	14.56	4.87
				Zn^+	11.732	0.153	7.69	3.42
				Ni^+	13.149	0.040	15.48	1.47
				S^+	14.421	0.065	12.72	2.42
6	2.625289	0.3	−26	Si^+	15.129	0.024	8.75	0.45
				Fe^+	14.700	0.016	11.38	0.38
				C^+	16.212	8.658	11.10	23.77
				N^0	14.789	0.017	14.08	0.58
				Al^+	13.537	1.752	5.32	4.91
				Zn^+	12.221	0.060	11.06	2.04
				Ni^+	13.463	0.019	12.19	0.59
				Cr^+	12.991	0.094	13.78	3.83
				S^+	14.786	0.035	10.78	0.79
				Ar^0	13.307	0.028	9.26	1.04
7	2.625612	0.1	+0	Si^+	15.057	0.014	9.77	0.37
				C^+	17.831	1.661	8.07	4.93
				N^0	14.627	0.018	5.93	0.26
				Al^+	14.132	0.622	9.25	2.24
				S^+	14.740	0.126	7.62	1.34
				Ar^0	13.432	0.021	8.49	0.67
8	2.625644	0.2	+3	Fe^+	14.473	0.010	8.46	0.21
				Ni^+	13.208	0.019	7.08	0.51
				Cr^+	12.826	0.110	7.89	2.73
9	2.625914	0.3	+25	Si^+	14.216	0.067	4.29	0.41
				Fe^+	13.602	0.019	7.80	0.47
				Al^+	12.501	0.157	3.48	1.15
				Ni^+	12.498	0.097	9.41	3.10
				S^+	14.479	0.540	23.68	32.07
10	2.625975	8.1	+30	Si^+	13.240	0.568	8.87	4.92
				C^+	14.161	0.542	7.22	4.70
				Al^+	12.087	0.562	7.65	4.22
11	2.626142	19.9	+44	Si^+	12.784	0.533	17.23	9.25
				C^+	13.499	1.107	14.30	16.84
				Al^+	11.560	0.479	18.75	12.47

[a]Velocity relative to z=2.62561

NOTE. — Portions of the C II 1334 and Al II 1670 transitions are heavily saturated in some velocity regions and column densities measured for these transitions are highly uncertain.

TABLE 3
IONIC COLUMN DENSITIES: INTERMEDIATE-IONS

ID	z_{abs}[a]	$\sigma(z)$ (10^{-5})	v_{rel}[b] (km/s)	Ion	$\log N$ (cm^{-2})	$\sigma(N)$	b[c] (km/s)	$\sigma(b)$
1	2.624360	0.0	−103	Al^{++}	12.264	0.049	11.64	1.07
2	2.624832	0.0	−64	Al^{++}	12.128	0.145	30.72	13.42
				N^{+}	13.909	0.162	30.72	0.00
				Fe^{++}	13.909	0.137	30.72	0.00
3	2.625035	0.0	−47	Al^{++}	12.922	0.051	15.87	1.32
				N^{+}	14.047	0.098	15.87	0.00
				Fe^{++}	13.919	0.056	15.87	0.00
4	2.625244	0.7	−30	Al^{++}	13.357	0.022	16.50	0.85
				N^{+}	14.764	0.045	16.50	0.00
				Fe^{++}	14.066	0.066	16.50	0.00
5	2.625612	0.0	+ 0	Al^{++}	12.629	0.157	5.27	0.89
				N^{+}	13.838	0.232	5.27	0.00
6	2.625697	6.5	+7	Al^{++}	12.429	0.285	10.79	3.05
				N^{+}	13.931	0.205	6.81	2.62
7	2.625914	0.0	+ 25	Al^{++}	12.105	0.058	9.29	0.70
				N^{+}	13.918	0.034	9.29	0.00
8	2.626142	0.0	+ 44	Al^{++}	11.710	0.329	27.48	26.17
				N^{+}	13.473	0.385	27.48	0.00

[a]Components 1–3,5,8,9 were fixed to have identical redshifts as components observed in the low-ion profiles.
[b]Velocity relative to z=2.62561
[c]Components with identical b values were tied together in the fit. In this case, an error is listed for only one component.

of damped Lyα profiles (e.g. Prochaska & Wolfe 1996), we found a significant improvement in χ^2 if the Doppler parameters were left untied from ion to ion. Even more unusual, however, is an observed offset in the $v \approx 0$ km/s component between the Fe II, Ni II, and Cr II transitions and the other low-ion transitions. We found a significant improvement in χ^2 if we fit the former transitions with a velocity component offset by +3 km/s. We have experimented with our VPFIT solution and have been able to shift the centroids of the Ni II and Fe II components by $\approx$ 1 km/s closer to the other ions by introducing another velocity component at $v \approx 10$ km/s. The resulting fit, however, is not a significant improvement in χ^2 over the present solution. We are concerned with this offset, in particular its implications for analyses which are extremely sensitive to such effects (e.g. Webb et al. 2001). It would have only a small impact on the current analysis, however, and we proceed under the assumption that all of the gas near $v = 0$ km/s has the same velocity.

2.2. *Intermediate-Ion Profiles*

We present a series of intermediate-ion profiles in Figure 2 which includes transitions of Fe^{++}, Si^{++}, Al^{++}, and N^{+}. To facilitate comparison with the low-ion transitions, we also plot the Si II 1808 transition. With the exception of Al III 1854, the profiles are located within the Lyα forest and may be contaminated by coincident Lyα clouds (we are confident that the dotted regions in Figure 2 are blends). For this reason, one may consider these column density measurements as upper limits except in the case where the profiles are heavily saturated and a precise estimate is impossible. We have fit these transitions with the VPFIT software package except Si III 1206 which we found to be too saturated to include in the analysis. If this ion has a similar component structure to the other

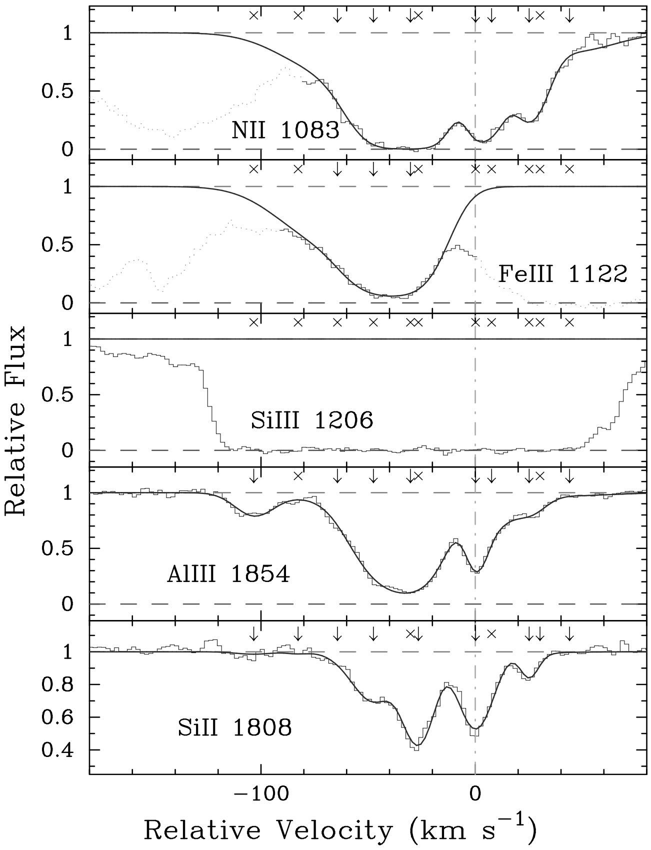

FIG. 2.— Same as Figure 1 but for the intermediate-ion transitions. For comparison, we also include the Si II 1808 low-ion profile.

intermediate-ions, then the majority of components have $N(\mathrm{Si}^{++}) > 10^{14}\,\mathrm{cm}^{-2}$. We adopt this limit throughout.

Similar to Figure 1, the marks at the top of each panel indicate the velocity centroids of the components included in the analysis with the arrows identifying the specific components included for a given ion. As described below, it is an analysis of these ions along with the low-ions which places the tightest constraints on the ionization state of the damped Lyα system. Therefore, we have attempted to fit the intermediate-ions with the line-profile solution obtained from the low-ion transitions, i.e., the components are placed at the same velocities as the low-ion solution. We achieved a satisfactory fit for the intermediate-ion profiles except at $v \approx -26$ km/s and $v \approx +8$ km/s. At $v \approx -26$ km/s, the χ^2 of the fit was significantly improved if the velocity component was offset by -4 km/s from the respective low-ion feature. We contend this offset is a physical effect and its implications on our photoionization modeling are discussed below. Meanwhile, we had to introduce a new component at $v \approx 8$ km/s to account for significant absorption at that velocity in the intermediate-ions. Table 3 presents the full solution for the intermediate-ion profiles.

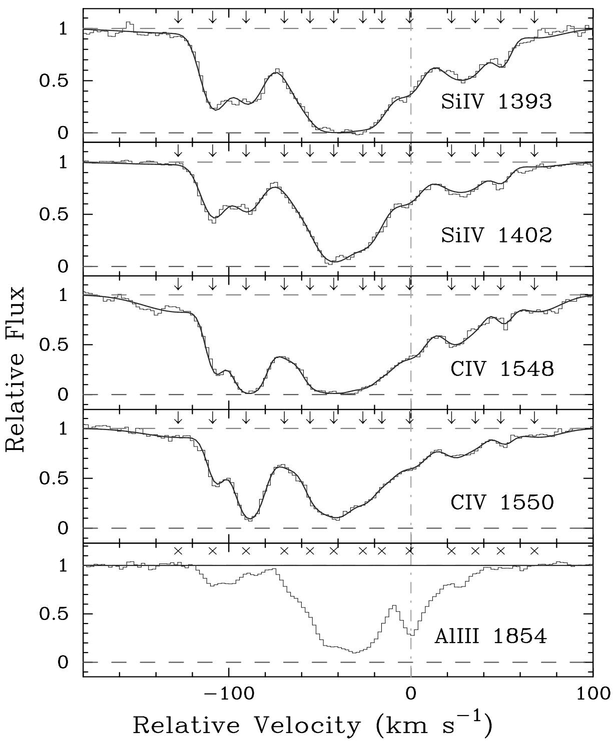

FIG. 3.— Same as Figure 1 but for the high-ion transitions. For comparison, we also include the Al III 1854 intermediate-ion profile.

2.3. *High-Ion Profiles*

In Figure 3, we present the profiles and VPFIT solution for the high-ion Si IV and C IV transitions. We have tied the redshifts of the velocity components for the two ions but have allowed the b-values to vary. We chose to fit the profiles independently of the low and intermediate-ions – even though several of the velocity components have similar redshifts – because we believe the high-ion gas is spatially separated from the low-ion gas (Wolfe & Prochaska 2000). For comparison, we plot an intermediate-ion Al III transition to emphasize its likeness to the Si IV profiles. The parameters of the solution are listed in Table 4.

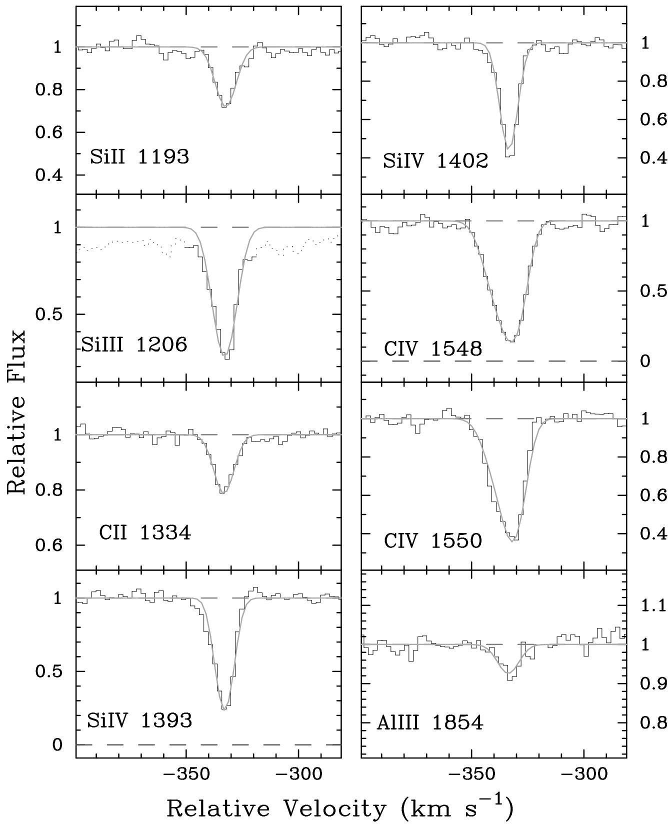

FIG. 4.— Velocity profiles of metal-line transitions from an absorption system associated with the $z_{abs} = 2.62$ damped Lyα system toward GB1759+7539. This system has very simple kinematics, suggesting the multiple ionic species arise in a single phase of gas. Most of the transitions are overplotted with a profile fit derived with the VPFIT software package (Table 5). Known blends have been dotted out in the figure.

2.4. $v \approx -330$ km/s *Feature*

Finally, we analysed a single absorption feature at $v = -330$ km/s which exhibits significant Si^+, Si^{++}, Si^{3+}, C^+, C^{3+}, and Al^{++} absorption (Figure 4). We fit all of the profiles with a single component except C^{3+} whose asymmetric shape indicates two components. The centroids of all of the ions are at nearly identical velocity including the stronger component of the C IV profiles. The column densities for these ions are very accurately measured (Table 5) and they provide a precise examination of the ionization state of this gas.

2.5. *Summary*

Table 6 presents an observational summary of various ionic ratios and column densities for the majority of velocity components identified in the metal-line profiles. The

TABLE 4
IONIC COLUMN DENSITIES: HIGH-IONS

ID	z_{abs}	$\sigma(z)$ (10^{-5})	v_{rel} (km/s)	Ion	$\log N$ (cm^{-2})	$\sigma(N)$	b (km/s)	$\sigma(b)$
1	2.624064	6.6	-127	C^{3+}	13.082	0.097	27.54	5.58
2	2.624293	0.3	-108	C^{3+}	13.335	0.036	5.27	0.50
				Si^{3+}	13.078	0.043	7.99	0.32
3	2.624515	0.4	-90	C^{3+}	13.997	0.020	8.16	0.48
				Si^{3+}	13.062	0.474	9.74	2.39
4	2.624769	4.4	-69	C^{3+}	13.344	0.287	9.51	5.39
				Si^{3+}	12.671	2.049	19.34	28.56
5	2.624940	4.1	-55	C^{3+}	13.426	1.201	6.74	4.60
				Si^{3+}	13.224	0.302	13.23	10.95
6	2.625097	2.7	-42	C^{3+}	14.084	0.462	11.57	11.85
				Si^{3+}	13.721	0.156	9.49	1.45
7	2.625291	2.4	-26	C^{3+}	13.467	1.444	6.61	8.54
				Si^{3+}	13.419	0.297	9.62	4.71
8	2.625417	11.5	-15	C^{3+}	13.374	0.943	7.92	8.63
				Si^{3+}	13.020	1.713	13.49	47.17
9	2.625601	5.8	0	C^{3+}	13.390	0.296	10.82	5.37
				Si^{3+}	12.830	1.236	9.37	4.35
10	2.625880	2.9	$+22$	C^{3+}	13.199	0.117	9.86	2.53
				Si^{3+}	12.847	0.199	12.26	5.16
11	2.626038	2.8	$+35$	C^{3+}	12.676	0.341	7.13	3.59
				Si^{3+}	12.508	0.336	9.39	4.50
12	2.626206	1.0	$+49$	C^{3+}	12.603	0.106	5.01	1.38
				Si^{3+}	12.341	0.137	5.09	1.02
13	2.626430	0.5	$+68$	C^{3+}	12.847	0.047	16.30	2.08
				Si^{3+}	12.236	0.065	18.97	3.30

TABLE 5
IONIC COLUMN DENSITIES: $v = -330$KM/S COMPONENT

Ion	z_{abs}	$\sigma(z)$ (10^{-5})	v_{rel} (km/s)	$\log N$ (cm^{-2})	$\sigma(N)$	b (km/s)	$\sigma(b)$
C^{+}	2.621580	0.6	-332	12.775	0.035	4.36	0.96
C^{3+}	2.621484	12.1	-340	13.030	0.876	6.62	5.17
C^{3+}	2.621580	3.0	-332	13.455	0.337	5.45	1.33
Si^{+}	2.621590	0.5	-332	12.387	0.031	4.64	0.85
Si^{++}	2.621584	0.3	-332	12.526	0.028	5.00	0.44
Si^{3+}	2.621570	0.1	-333	12.956	0.016	3.54	0.15
Al^{++}	2.621571	0.8	-333	11.537	0.112	5.39	2.39
Al^{+}	...	...	-333	< 10.8			

TABLE 6
SUMMARY TABLE

Ratio	−333	−105	−65	−47	−26	0	25
C^{3+}/C^+	0.80	−0.97	< -1.67	...	< -2.95	< -4.45	...
Si^{3+}/Si^+	0.56	−0.37	−0.83	−1.18	−1.71	−2.23	−1.37
Al^{++}/Al^+	> 0.74	> -0.73	−0.26	< -0.49	< -0.29	−1.50	−0.40
N^+/N^0	...	...	> 0.21	−0.35	−0.02	−0.79	...
Fe^{++}/Fe^+	...	...	0.46	−0.41	−0.63	< -1.88	...
Si^{++}/Si^+	0.12	> 0.15	...	...	...	...	...
Fe^{++}/Al^{++}	...	...	1.78	1.00	0.71	< -0.04	...
Fe^{++}/N^+	...	...	0.00	−0.13	−0.70	< -1.25	...
$[Al^{++}/Si^+]$	0.22	−0.12	−0.31	−0.91	−0.70	−1.36	−1.04
$[Ar^0/S^+]$	...	...	...	...	−0.80	−0.63	...
$[Si^+/Fe^+]$	...	...	−0.01	0.51	0.37	0.52	0.55
$[Ni^+/Fe^+]$	...	...	...	0.07	0.01	−0.02	0.15
$[S^+/Fe^+]$	...	...	...	0.39	0.39	0.57	1.18
$[Cr^+/Fe^+]$	...	...	...	...	0.12	0.18	...
$[Zn^+/Fe^+]$	...	...	...	0.23	0.35	...	...
$[N^0/S^+]$	...	...	...	−0.79	−0.77	−0.88	...
$[N^0/Si^+]$	...	...	< -0.21	−0.91	−0.75	−0.84	...
$[Fe^{++}/Al^{++}]$	...	...	0.77	−0.01	−0.30	< -1.05	...
$\%[N_{TOT}(Si^+)]$	0.1	0.8	0.9	22.5	37.9	32.2	4.6
$\%[N_{TOT}(S^+)]$	...	...	...	15.3	35.4	31.9	17.5
$\%[N_{TOT}(Fe^+)]$	...	...	2.6	19.8	46.4	27.5	3.7
$\%[N_{TOT}(Fe^{++})]$	...	...	28.5	29.2	40.9	< 1.4	...
$\%[N_{TOT}(Al^{++})]$	0.8	4.2	3.1	19.3	52.5	9.8	2.9
$\%[N_{TOT}(N^+)]$	...	...	7.8	10.7	55.8	6.6	8.0
$\%[N_{TOT}(N^0)]$	...	...	< 3.7	18.8	45.9	31.6	...

velocities listed at the top of the Table designate 10 km/s bins where all of the gas within 5 km/s of the centroid has been summed for the ionic column densities. All ratios are logarithmic values with the square bracket notation indicating values relative to solar abundances, i.e., $[X/Y] \equiv \log(N(X)/N(Y)) - \log(X/Y)_\odot$.

3. ANALYSIS OF THE GAS AT $v < -50$ km/s

In this section we consider various diagnostics on the ionization state of the gas at $v < -50$ km/s along the sightline. It is important to keep in mind that the absorption at any velocity may be the result of several components which simply overlap in velocity space. These components might each have a unique set of physical characteristics (e.g. metallicity, ionization state) and therefore comparisons of different ions at a given velocity may be open to several interpretations.

3.1. *Gas at* $v \approx -330$ km/s

As revealed by Figure 4, there is an absorption feature at $v \approx -330$ km/s which exhibits significant absorption for many ions: Si^+, Si^{++}, Si^{3+}, C^{3+}, C^+, and Al^{++}. The kinematic structure is very simple and we fit the profiles with a single component (Table 5). In fact, the feature is so simple that we are confident the majority of gas is spatially well-localized. The Si^{3+}, C^{3+}, and Al^{++} ions have significantly higher column densities than their low-ion counterparts indicating the gas is highly ionized. Significant Si^{3+} and C^{3+} column densities can arise from a number of physical processes including collisional ionization and photoionization by high energy photons. Because the observed Doppler parameters are small, we place a 2σ upper limit on the temperature independently from the C^+ and Si^{3+} measurements: $T < 3 \times 10^4$ K. In turn, this indicates the gas is not in collisional ionization equilibrium because $T \gtrsim 4 \times 10^4$ K is required to produce significant amounts of C^{3+} (c.f. Sutherland & Dopita 1993). This naturally suggests the ionization may be dominated by photoionization.

Although this system is well separated by velocity from the damped Lyα system, its characteristics are important for several reasons. First, it is possible that this gas is representative of the gas giving rise to the C IV and Si IV profiles presented in Figure 3. Therefore, the gas responsible for the C IV and Si IV profiles makes a negligible contribution to the low-ion column densities – and presumably N(HI) – of the damped Lyα system. A similar conclusion has been inferred from the observed differences in the low and high-ion profiles of many other damped Lyα systems (Lu et al. 1996; Wolfe & Prochaska 2000). We also note that the Si^{++}/Si^{3+} and Al^{++}/Si^{3+} ratios are sufficiently small for the $v \approx -330$ km/s component that gas with its ionization characteristics cannot reproduce both the high and intermediate-ion column densities at $v \approx 0$ km/s. If we attribute the CIV and SiIV profiles at $v > -50$ km/s in Figure 3 to an ionized gas similar to the $v \approx -330$ km/s component, then we must introduce at least one additional phase of gas for the intermediate-ions *independent of the* *low-ions.* Therefore, if the intermediate and low-ions have distinct origins, this indicates the presence of three unique ionization phases at a similar velocity in this damped Lyα system.

The absorption feature at $v \approx -330$ km/s is further important because it poses a difficult challenge to ionization models. Because of its simple kinematics and low temperature, the gas is very likely in a single component with a single set of physical conditions. Equilibrium collisional ionization models or more exotic turbulent mixing layers (e.g. Shull & Slavin 1994) are inconsistent with the temperature of the gas. If the gas is in equilibrium, therefore, then we presume it has been photoionized.

With the range of ions and very accurate column densities observed, we expected to precisely constrain its ionization state. To this end, we performed a series of photoionization calculations using the CLOUDY software package with both an extragalactic UV background spectrum (Haardt & Madau 1996) and a series of Kurucz (1988) O-star spectra. We varied the HI column density of the plane-parallel 'cloud', assumed a range of metallicities, and calculated the ionization state at a range of ionization parameters,

$$U \equiv \frac{\phi}{c n_H} \gtrsim (2 \times 10^{-5}) \, \frac{J_{912}/10^{-21.5}}{n_H/\,\mathrm{cm}^{-3}} \quad , \tag{2}$$

where n_H is the volume density of hydrogen, ϕ is the surface flux of ionizing photons with $h\nu > 1$ Ryd, and J_{912} is the intensity of the incident radiation at 1 Ryd. The relation in Equation 2 approximately holds for ionizing radiation fields which steeply decline at energies greater than 1 Ryd.

To our surprise, we cannot identify any single-phase (e.g. constant density) photoionization model which can match the observed ratios of the Si ions ($\mathrm{Si^+ : Si^{++} : Si^{3+}} = 1 : 1.3 : 4$). The principal conflict is that models which predict $N(\mathrm{Si^+}) \approx N(\mathrm{Si^{++}})$ always require $N(\mathrm{Si^{++}}) > N(\mathrm{Si^{3+}})$ in stark contradiction with our observations. This difference between the predicted and observed ratios is generally greater than a factor of 10. It holds independently of the shape or flux of the input spectrum or any assumptions on the metallicity or H I column density. We also note that even if we allow the temperature to be a free parameter, it is impossible to reproduce the Si ionic ratios through a combination of collisional and photoionization. In conclusion, we contend *the gas cannot be described by a single ionization phase in equilibrium conditions.* While this could be a common occurrence in quasar absorption line systems, it is very surprising for this feature because of its simple kinematics.

Granted the failure of the single-phase equilibrium models, we also considered the prospect that the gas arises in two distinct phases with very different ionization states. If we combine a very neutral component with a highly ionized component, we approach the observed ratios of Si and C but still fail at the $> 95\%$ c.l. Furthermore, the best fitting model couples an extremely neutral gas with an extremely photoionized gas in a mixture of $\approx 2:1$, which would be unlikely given the extremely simple kinematics of the observed metal-line profiles. It would take a contrived set of physical conditions to couple two-phases of gas with such extreme ionization characteristics at identical velocities and both with $T < 3 \times 10^4$ K. Finally, this two-phase model predicts an O I column density in conflict with our observed upper limit. To this end, we have failed to appropriately model the ionization state of this velocity component. Although it has no direct bearing on our damped Lyα analysis because of its very small metal content, we interpret this failure as a stern warning for the challenges associated with making ionization corrections for highly ionized gas.

Our photoionization models do not accurately predict the ionization structure of the -330 km/s complex; furthermore, collisional ionization equilibrium models cannot provide the required ionization since the upper limits on the kinetic temperature ($T < 3 \times 10^4$ K) are too small to allow collisional production of C IV and Si IV in great quantities (Sutherland & Dopita 1993). It is possible that the gas in this component is not in ionization equilibrium. Non-equilibrium ionization can occur, for example, if the cooling time of shock-heated gas is significantly longer than the recombination time (Shapiro & Moore 1976; Sutherland & Dopita 1993). Models of time-dependent ionization of hot gas (e.g., gas hot enough to produce significant amounts of the highly-ionized species observed in this cloud) generically predict much larger ionization fractions of highly-ionized species at the temperatures appropriate for this component than do equilibrium models. Thus another potentially valid model for the -330 km/s gas is that this component was initially shock-heated to high temperatures ($T > 10^5$ K) and has cooled relatively quickly, with its ionization state lagging its temperature. While the ionization fractions of $\mathrm{C^{3+}}$ and $\mathrm{Si^{3+}}$ can be large even to temperatures as low as 10^4 K in such scenarios (Sutherland & Dopita 1993), we note that models of non-equilibrium ionization balance are dependent upon the initial conditions of the gas. Thus it is difficult to determine if the ionization structure of the -330 km/s absorption is consistent with this non-equilibrium scenario without unfounded guesses at its initial temperature, density, and abundance.

3.2. *Gas at $v \approx -105$ and -65 km/s*

The low column density gas with $v \approx -105$ and -65 km/s exhibits significantly different ionization characteristics than the $v \approx -330$ km/s component. Although the ionic ratios (e.g. $\mathrm{Si^{++}/Si^+}$, $\mathrm{Fe^{++}/Fe^+}$, and $\mathrm{N^+/N^0}$) all indicate the gas is predominantly ionized ($x \approx 1$), the $\mathrm{C^{3+}}$ and $\mathrm{Si^{3+}}$ ions comprise a much smaller fraction of the elemental column densities than the $v \approx -330$ km/s component.

The properties of the gas at $v \approx -65, -105$ km/s may have important implications for the intermediate-ion gas observed at $v > -50$ km/s. Consider the possibility that the low and intermediate-ion profiles at $v > -50$ km/s arise from two ionization phases: (i) a neutral gas phase and (ii) a highly ionized gas with properties similar to the gas at $v \approx -65, -105$ km/s. In this case, we can estimate the contribution of this ionized phase to the total $\mathrm{Fe^+}$ column density at $v > -50$ km/s from the following treatment. At $v \approx -65$ km/s, we measure a $\mathrm{Fe^{++}/Fe^+}$ ratio of $+0.46$ dex. If we assume the same ratio applies at $v \approx -26$ km/s, then the $N(\mathrm{Fe^{++}})$ value at $v \approx -26$ km/s implies $N(\mathrm{Fe^+}) = 10^{14}\,\mathrm{cm^{-2}}$ which is $\approx 20\%$ of the total $N(\mathrm{Fe^+})$ value at that velocity. Therefore, an ionized gas component could comprise roughly 20% of the low-ion absorption observed at $v \approx -26$ km/s. We develop this treatment to much greater depth in the following section.

4. ANALYSIS OF THE LOW-ION REGIONS AT $v > -50$ km/s

The three velocity components at $v \approx -47, -26$, and 0 km/s comprise nearly all of the low-ion gas in this damped Lyα system. In terms of the system's chemical abundances, therefore, ionization corrections on the column densities derived from the low-ion profiles at these velocities are the most important.

4.1. $v \approx 0$ km/s

It is most instructive to begin with the $v \approx 0$ km/s component where, initially, there are conflicting photoionization diagnostics. On the one hand, the Ar^0/S^+ ratio is significantly sub-solar which indicates the majority of Ar is ionized (e.g. Sofia & Jenkins 1998): $[Ar^0/S^+] \approx -0.7$ dex. Therefore, one might expect photoionization is significantly affecting the chemical abundances inferred from all of the low-ion transitions. On the other hand, we have placed a strict upper limit on the Fe^{++} column density which limits the level of photoionization of this gas. The adopted limit of $\log N(Fe^{++}) < 12.6$ dex results from the low optical depth observed at $v \approx 0$ km/s in the Fe III 1122 profile (Figure 2). We stress that the absorption present at $v \approx 0$ km/s is probably due to an intervening Lyα cloud and therefore the $N(Fe^{++})$ value is possibly lower than $10^{12}\,cm^{-2}$. Even adopting our more conservative upper limit, $Fe^{++}/Fe^+ < -1.9$ dex (Tables 2,3), this indicates the gas has a small ionization fraction. Finally, the moderate strength charge-exchange reactions between N and H which roughly couple the column densities of N^0, N^+, H^0, and H^+, allow one to crudely estimate the ionization fraction of hydrogen from the observed N^+ and N^0 column densities. We find $N^+/(N^+ + N^0) \approx 0.15$ which suggests $x \approx 15\%$, although N can be modestly overionized with respect to hydrogen because of its larger ionization cross-section. We contend a similar effect explains the sub-solar Ar^0/S^+ ratio observed for this predominantly neutral gas.

To perform a quantitative analysis of photoionization, we have performed a series of calculations with the CLOUDY software package. We caution that the accuracy of these calculations are limited by a number of uncertainties associated with the physical nature of the absorbing gas and the incident ionization field. We consider here a series of single-phase, constant density models with varying ionization parameter, the Haardt-Madau spectrum, and assume $N(HI) = 10^{20}\,cm^{-2}$ which is roughly consistent with the relative strength of the low-ions and the total H I. In Figure 5, we plot the predicted logarithmic abundance of low-ion X_i relative to Fe^+ relative to the intrinsic abundance of these two elements,

$$[X_i/Fe^+] = \log(N(X_i)/N(Fe^+)) - \log(X/Fe)_\odot \quad , \qquad (3)$$

against the Fe^{++}/Fe^+ ratio. We focus on $[X_i/Fe^+]$ instead of $[X_i/H^0]$ because we are more concerned with the effects of photoionization on interpretations of relative elemental abundances [X/Y] instead of metallicity [X/H] in the damped Lyα systems. Departures of $[X_i/Fe^+]$ from zero indicate that photoionization corrections are required to calculate accurate elemental abundance ratios from the low-ion column densities independent of dust depletion. Positive (negative) $[X_i/Fe^+]$ values would imply overestimates (underestimates) of [X/Fe] from the low-ion ratios. Finally, the black dashed line plots the ionization fraction, $\log x$, on the same logarithmic scale.

At $Fe^{++}/Fe^+ < -1.9$ dex, we note $\log x < -1$ indicating the hydrogen gas is less than 10% ionized. Therefore, we are confident that the gas at $v \approx 0$ km/s is predominantly neutral. In turn, we find the ionization corrections are negligible for Si^+, Cr^+, and Ni^+ relative to Fe^+ and small for S^+, Al^+, and N^0. Only Ar^0 requires a large ionization correction which brings the corrected Ar/S ratio into closer agreement with the solar abundance. This gas resembles the β Cen A ISM sightline analysed by Sofia & Jenkins (1998) which shows similarly over-ionized Ar/S in a gas with a relatively large neutral hydrogen fraction. The fact that the inferred Ar/S ratio remains sub-solar even after the ionization corrections implied by Figure 5 may reflect differential depletion but more likely points to an error in our adopted ionization spectrum or possibly uncertainties in the atomic physics of Ar. In either case, the difference reflects an error in our photoionization modeling.

We emphasize that our conclusions on the ionization state of this gas are further supported by the low Al^{++}/Al^+ and Fe^{++}/Al^{++} ratios. Our results are also consistent with the observed Si^{++}/Si^+, Si^{3+}/Si^+, and C^{3+}/C^+ ratios. Furthermore, we have also considered a Kurucz stellar ionizing spectrum with $T = 30000 - 50000$ K and more complicated two-phase scenarios and have found no qualitative differences in these analyses. In conclusion, the gas at $v \approx 0$ km/s has a low ionization fraction ($x \ll 1$) and ionization corrections to the observed low-ion column densities are nearly negligible except in the case of Ar^0. Therefore, the chemical abundances for this gas are accurately represented by the low-ion species.

4.2. $v \approx -26$ *and* -47 km/s

Now consider the gas at $v \approx -47$ and -26 km/s which exhibits significantly larger N^+/N^0, Al^{++}/Al^+, and Fe^{++}/Fe^+ ratios than the gas at $v \approx 0$ km/s. In the case of N^+ and Fe^{++}, we stress that these transitions lie in the Lyα forest and may suffer from contamination by coincident Lyα clouds. In the following, we proceed under the assumption that such contamination is small. Making a crude estimate of the ionization fraction from the observed N^+/N^0 ratio as above, we find $x \approx 50\%$ assuming $N^+/N^0 \approx -0.1$ dex. We also note that the Al^{++}/Si^+ ratios are high relative to the majority of damped Lyα systems (Vladilo et al. 2001). Altogether, we expect this gas to be more highly ionized than the $v \approx 0$ km/s component.

The greatest challenge in accurately assessing the impact of photoionization in the damped Lyα systems is our ignorance of the physical nature of the gas 'clouds' responsible for the absorption. We have no *a priori* knowledge of the metallicity, HI column density, volume density, or the underlying nucleosynthetic or dust depletion patterns. Furthermore, the absorption at any velocity could very well be the superposition of many clouds each with a unique set of physical characteristics but coincident velocity along the sightline. As such, there may be several

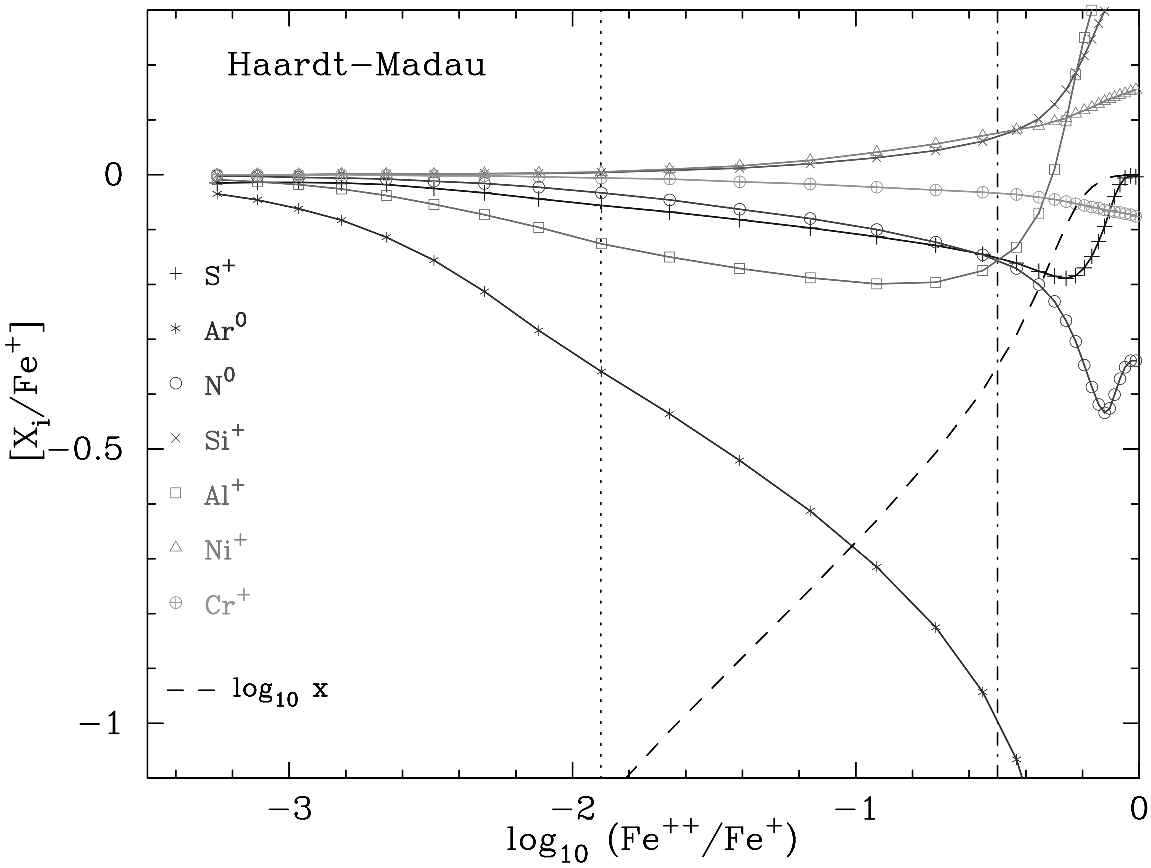

FIG. 5.— Predicted logarithmic abundance of low-ion X_i relative to Fe^+ relative to the intrinsic abundance of these two elements (Equation 3) against the Fe^{++}/Fe^+ ratio. Departures of $[X_i/Fe^+]$ from zero indicate that photoionization corrections are required to calculate accurate elemental abundance ratios from the low-ion column densities independent of dust depletion. Positive (negative) $[X_i/Fe^+]$ values would imply overestimates (underestimates) of [X/Fe] from the low-ion ratios. The black dashed line plots the ionization fraction, $\log x$, on the same logarithmic scale as $[X_i/Fe^+]$. For this analysis, we have assumed the Haardt-Madau spectrum, N(HI) = 10^{20} cm^{-2}, and [Fe/H] = –1. All of these quantities were derived with the CLOUDY software package.

clouds with different ionization states giving rise to the various metal-line profiles. Our approach is to consider simplest models first and then qualitatively assess the effects of more sophisticated scenarios.

We consider the two following cases: (1) the gas arises in a single cloud with one ionization phase; and (2) the gas arises in two gas clouds with very different degrees of ionization and possibly metallicity. Before proceeding, we present a line of circumstantial evidence that the ionization corrections to the elemental abundances might be small for this gas. In Table 6, we note that the relative abundances of the low-ion species of S, N, Ar, Si, Fe, Ni, and Cr are relatively uniform over all of these low-ion components. In all cases, the ratios vary by less than 0.2 dex from component to component. If one adopts the unfounded assumption that the gas in the entire damped Lyα system shares similar elemental abundances, then one would infer that the ionization corrections are small. Conversely, significant ionization corrections might require large abundance variations, possibly from different chemical enrichment histories or dust depletion patterns.

4.2.1. *Single Phase Model*

The simplest scenario is that the gas is contained within a single, constant density cloud with one ionization phase[6]. If the cloud is subjected to an external radiation field, there will be a radial variation in the degree of ionization of the gas; the outer layers are highly ionized and the inner regions are primarily neutral. With the exception of Al^{++} (e.g. Prochaska & Wolfe 1996), the intermediate-ions arise in the outer layers of the cloud because few high energy photons reach the inner regions. In this important respect, the single-phase model mimics the two-phase scenarios presented next. Because the N^+/N^0, Fe^{++}/Fe^+, and Fe^{++}/Al^{++} ratios are similar for the gas at $v \approx -26$ and -47 km/s, we consider the two components together. The uncertainties in our photoionization modeling presumably exceed any differences in the ionic column densities of the two velocity components.

Our analysis relies on simulations drawn from the CLOUDY software package. Figure 6 presents the predicted column densities N(X) for a series of ionization parameters assuming $N(\mathrm{HI}) = 10^{20}\,\mathrm{cm}^{-2}$, a metallicity [Fe/H] $= -1$, and the Haardt-Madau EUVB spectrum at $z = 2.5$. The H I column density and metallicity are reasonably consis-

[6] This treatment is identical to the scenario envisioned by Prochaska & Wolfe (1996) and the model designated H1 by Vladilo et al. (2001).

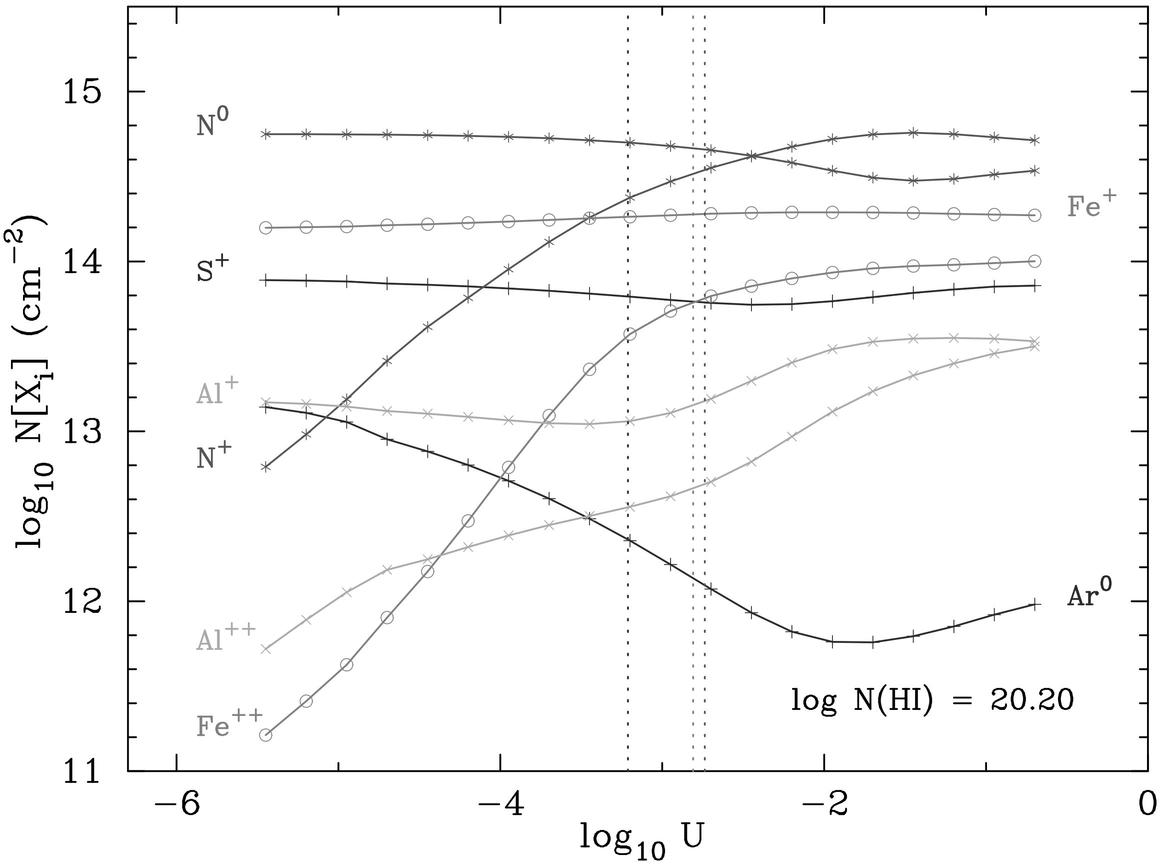

FIG. 6.— Predicted column densities $N(\mathrm{X})$ for a series of ionization parameters assuming $N(\mathrm{HI}) = 10^{20}\,\mathrm{cm}^{-2}$, a metallicity [Fe/H] = −1, and the Haardt-Madau EUVB spectrum at $z = 2.5$. The vertical dashed lines indicate the observed ratios of $\mathrm{Fe}^{++}/\mathrm{Fe}^{+}$, $\mathrm{N}^{+}/\mathrm{N}^{0}$, and $\mathrm{Ar}^{0}/\mathrm{S}^{+}$ and we note that the $\mathrm{Al}^{++}/\mathrm{Al}^{+}$ upper limit is consistent requires $\log U < -2$ dex. We find that all four of these ionization diagnostics are consistent with a single ionization phase and $\log U \approx -3$ dex.

tent with the total quantities inferred from the entire system. We emphasize that at $N(\mathrm{HI}) \gtrsim 10^{20}\,\mathrm{cm}^{-2}$, the exact $N(\mathrm{HI})$ value that one assumes has little impact on the single-phase scenarios. We also note that the $N(\mathrm{X})$ values presented in Figure 6 are less important than the relative values of the pairs of lines with identical color and symbols (e.g. $\mathrm{Fe}^{++}/\mathrm{Fe}^{+}$). The vertical dashed lines indicate the observed ratios of $\mathrm{Fe}^{++}/\mathrm{Fe}^{+}$, $\mathrm{N}^{+}/\mathrm{N}^{0}$, and $\mathrm{Ar}^{0}/\mathrm{S}^{+}$ and the $\mathrm{Al}^{++}/\mathrm{Al}^{+}$ upper limit requires $\log U < -2$ dex. We find that all four of these ionization diagnostics are consistent with a single ionization phase where $\log U \approx -3$ dex. The agreement is not perfect, but it is acceptable given the number of assumptions and uncertainties in the photoionization modeling. For example, a slightly softer ionizing spectrum would help bring the predicted $\mathrm{Ar}^{0}/\mathrm{S}^{+}$ ratio into better agreement with the observations at $\log U \approx -3$ dex.

The implications of the single phase model with $\log U \approx -3$ are as follows. First, we derive an ionization fraction $x \approx 50\%$ which indicates the gas is partially ionized. Second, if the metallicity of the velocity components at $v > -50$ km/s is constant, then the $v \approx -26$ km/s component may exhibit a larger $N(\mathrm{H})$ value than the gas at $v \approx 0$ km/s. Third, the degree of photoionization is significant enough to imply ionization corrections to the relative abundances derived solely from the low-ion species. Referring to Figure 5, one notes that as $\mathrm{Fe}^{++}/\mathrm{Fe}^{+} \to 0$ dex several of the low-ion ratios $[\mathrm{X}_i/\mathrm{Fe}^{+}]$ require modest ionization corrections. With the exception of Ar^0, the corrections are generally small (< 0.3 dex) but significant compared to the typical statistical errors in these measurements. The vertical black dash-dot line in Figure 5 indicates the approximate observed $\mathrm{Fe}^{++}/\mathrm{Fe}^{+}$ value of −0.5 dex. For this value, the low-ion ratios overestimate Si and Ni relative to Fe by ≈ 0.1 dex while Al, S, and N are underestimated by ≈ 0.2 dex. These ionization corrections are relatively small, but can have important implications for the relative elemental abundances of the damped Lyα systems. For example, correcting the S and Si abundances gives [S/Si] and [Si/Fe] values for the $v \approx -26$ km/s component which differ by ≈ 0.3 dex from the $v \approx 0$ km/s gas. One concludes, therefore, that the relative elemental abundances may differ significantly within this damped Lyα system.

We have also considered a single-phase model with the Kurucz stellar ionizing spectrum and a range of stellar effective temperatures. These models imply similar corrections; compare against Figure 7 which plots a $T = 40000$ K model with $N(\mathrm{HI}) = 10^{20}\,\mathrm{cm}^{-2}$. The principle differences are that $[\mathrm{Cr}^{+}/\mathrm{Fe}^{+}]$ shows a large offset from solar and that $[\mathrm{S}^{+}/\mathrm{Fe}^{+}]$ is positive at high $\mathrm{Fe}^{++}/\mathrm{Fe}^{+}$ values and significantly negative at $\mathrm{Fe}^{++}/\mathrm{Fe}^{+} < -2$ dex. These differences arise from the softer Kurucz ionizing spectra (e.g. a signif-

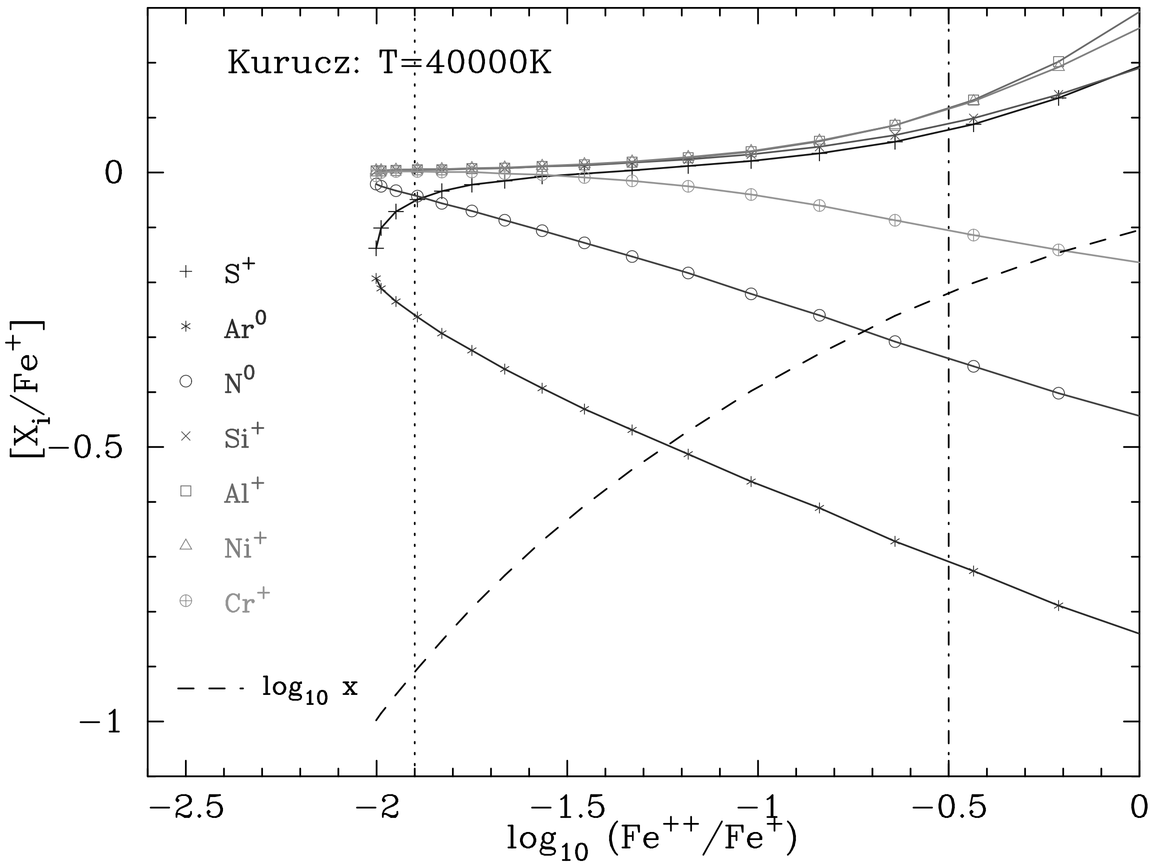

FIG. 7.— Predicted logarithmic abundance of low-ion X_i relative to Fe^+ relative to the intrinsic abundance of these two elements against the Fe^{++}/Fe^+ ratio. The analysis and presentation is identical to Figure 5 except the ionizing spectrum is a Kurucz $T = 40000$ K stellar model.

icant fraction of S is in S^0 at low ionization potential) and they highlight the uncertainties in our models related to the assumed input spectrum. In theory, one might observe enough ions to discriminate between various ionizing spectra but in practice one must allow for these uncertainties.

4.2.2. *Two-Phase Model*

Although we found that the single-phase scenario gave reasonable agreement to our set of photoionization diagnostics, we also wish to investigate the effects of a two-phase scenario. In particular, we want to determine if the two approaches yield different estimates for the ionization corrections (e.g Vladilo et al. 2001). We will show that the two models predict similar corrections but with important differences for S^+ and Ar^0.

Consider the following scenario where the low and intermediate-ions arise in two parcels of gas with unique ionization characteristics. As discussed in § 3.2, it is possible that gas with properties similar to the ionized gas at $v \approx -65$ km/s is entirely responsible for the intermediate-ions but also contributes a significant percentage of the low-ion column densities. In fact, we estimated an ionized component could contribute $\approx 20\%$ of the Fe^+ gas observed at $v \approx -26$ km/s. This scenario resembles the physical conditions along the sightline to HD 93521 in the Galactic ISM, where Sembach et al. (2000) describe the impact of the Warm Ionized Medium on measuring elemental abundances. For the damped system, a multiphase interpretation is further supported by an observed offset between the low and intermediate-ion gas at $v \approx -26$ km/s. Examining Tables 2 and 3, one notes that the component which best describes the low-ion gas at $v \approx -26$ km/s is offset by ≈ 4 km/s from the centroids of the Al^{++}, N^+, and Fe^{++} component. The difference is relatively small and may be the result of a systematic error, but we consider it more likely that the gas at $v \approx -26$ km/s is best described by at least two components with very different ionization fractions[7]. In any case, because the offset is small one must consider the impact of the ionized gas on the observed low-ion column densities and we treat the two clouds as if they had identical velocities. This treatment is similar to the scenario introduced by Howk & Sembach (1999) and extended by Vladilo et al. (2001).

Consider the following model which assumes the gas at $v \approx -26$ km/s is comprised of two components: (i) a very neutral component (e.g. $Fe^{++}/Fe^+ \ll 1$) and; (ii) an ionized component with identical relative gas-phase abundances that contributes all of the intermediate-ions observed at $v \approx -30$ km/s. Even though the latter component is significantly ionized, it may still exhibit signifi-

[7] Unfortunately, the gas at $v \approx -47$ km/s is not precisely localized in velocity space and can be well described by a single or multiple clouds.

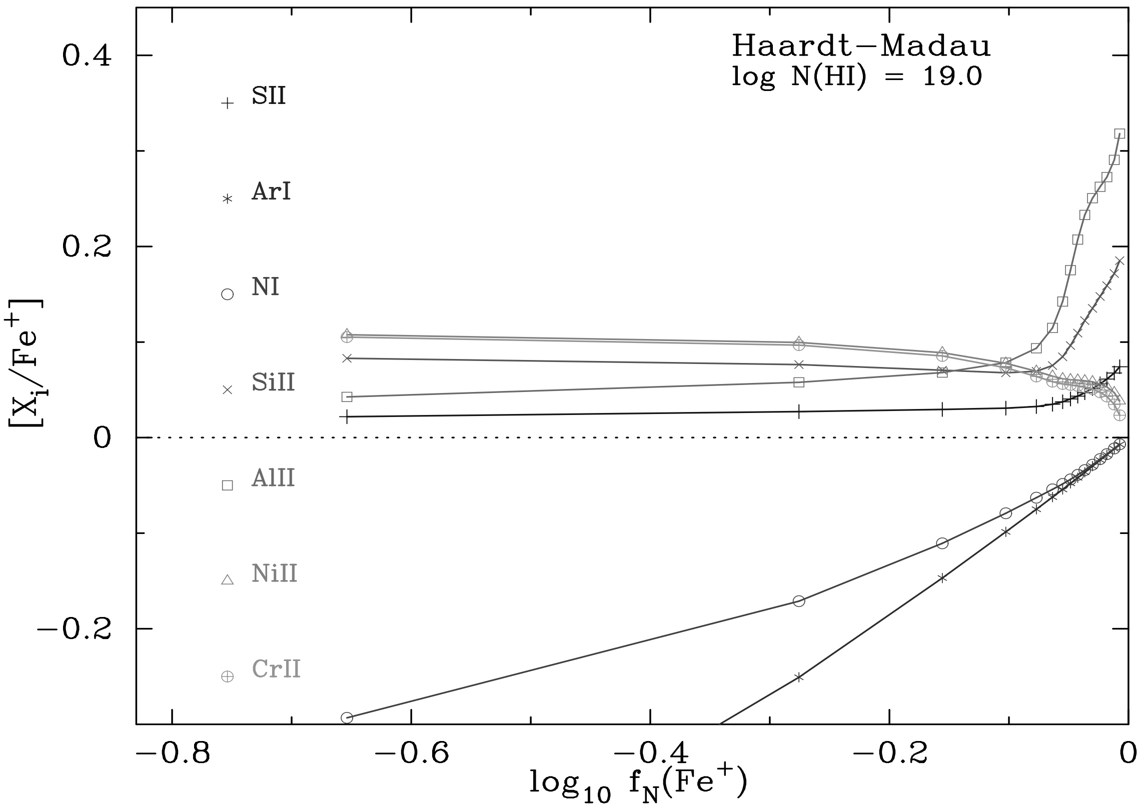

FIG. 8.— Offsets from the intrinsic abundances of low-ion X_i relative to Fe^+, $[X_i/Fe^+]$, against the fraction of Fe^+ arising in the neutral component $f_N(Fe^+)$of our two-phase models. Similar to the single-phase models, the implied ionization corrections are small for the majority of elements although there are several quantitative differences. For this analysis, we have assumed the Haardt-Madau spectrum and that $N(\mathrm{HI}) = 10^{19}$ cm^{-2} for the ionized component

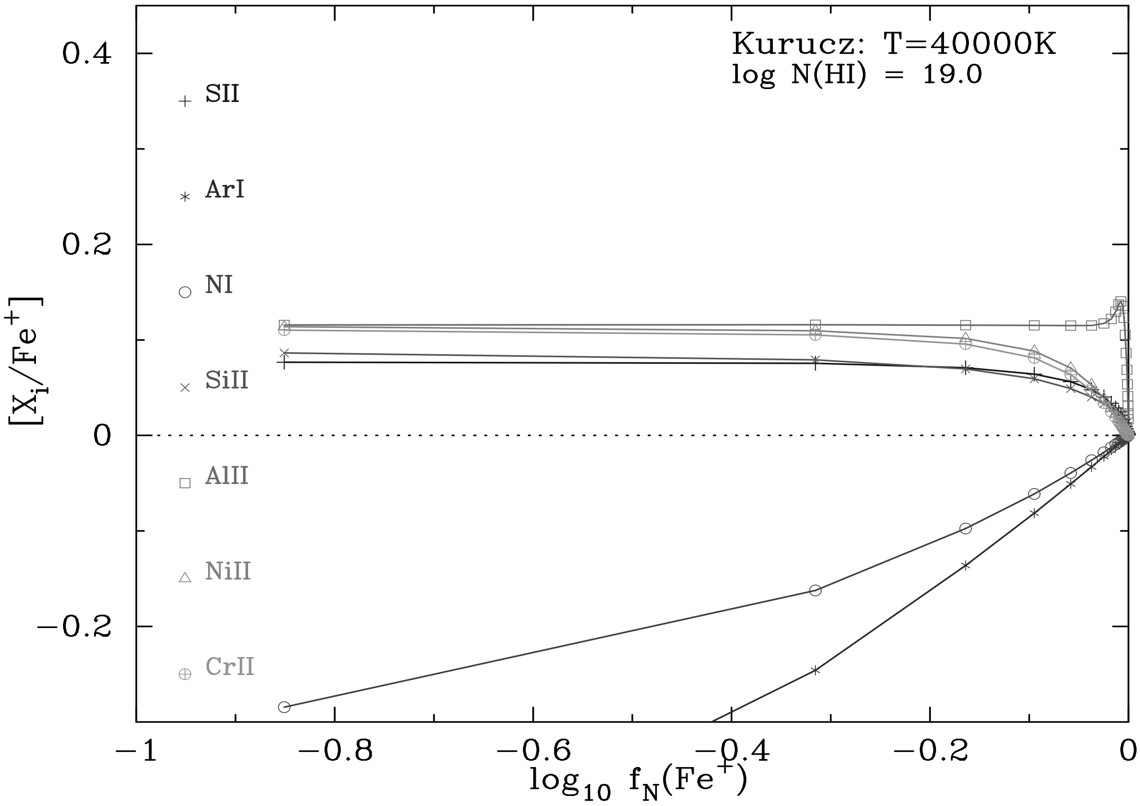

FIG. 9.— Same as Figure 8 except we have assumed a Kurucz (T = 40000 K) stellar model.

cant column densities of several low-ion species, (e.g. S^+, Si^+, and Al^+) and, therefore, impact the relative elemental abundances and metallicity derived from the low-ion transitions.

To illustrate the ionization corrections for this two-phase model we introduce a new parameter, $f_N(X_i) \equiv (X_i)_{neutral}/(X_i)_{total}$, which is the fraction of low-ion X_i that is attributed to the neutral gas component. We have used CLOUDY calculations similar to those presented in the previous section to calculate the ionization state of the ionized component but assuming the HI column densities are lower than $10^{20}\,\mathrm{cm}^{-2}$. In this case the ionized component contributes a small fraction of the total HI column density. We constrain the two-phase model by requiring that it yields a Fe^{++}/Fe^+ ratio of -0.5 dex. Because this constraint refers to a relative abundance instead of the absolute Fe^{++} and Fe^+ column densities, our analysis is not very sensitive to the N(HI) value or metallicity assumed for the ionized component. Changing the N(HI) value for the ionized component by 0.5 dex can be important, however, and we consider the effects below.

We first present results assuming $N(\mathrm{HI}) = 10^{19}\,\mathrm{cm}^{-2}$ in the ionized component and adopting the Haardt-Madau spectrum. Figure 8 plots the offset from the intrinsic abundances of low-ion X_i relative to Fe^+, $[X_i/Fe^+]$, against the fraction of Fe^+ arising in the neutral component $f_N(Fe^+)$. As $f_N(Fe^+)$ increases in the figure, the ionized component contributes less Fe^+ and therefore there is a compensatory increase in the ionization state of this gas to match the observed Fe^{++}/Fe^+ ratio. At low $f_N(Fe^+)$ values, one approaches the single-phase model presented in the previous sub-section. Note that one derives a qualitatively similar set of results by examining $f_N(N^0)$ and constraining the predicted N^+/N^0 ratio by the observed value.

Similar to the single-phase model, the implied ionization corrections are small for the majority of elements although there are several quantitative differences. First, the offsets for $[S^+/Fe^+]$ are generally small or slightly positive whereas the single-phase model predicted negative offsets approaching -0.2 dex. The difference can be attributed to the difference in optical depth of the single-phase model and the ionized component in the two-phase scenario where we have assumed $N(\mathrm{HI}) = 10^{20}\,\mathrm{cm}^{-2}$ and $10^{19}\,\mathrm{cm}^{-2}$ respectively. In the former case, the self-shielding from H I is large enough that S is much less ionized relative to Fe. Second, the offsets for Ar^0/Fe^+ are small at all but the lowest $f_N(Fe^+)$ values. This is because we have assumed Ar is entirely in atomic form in the neutral component. If this two phase model is an accurate representation of the gas, the neutral component must have a sub-solar Ar^0/S^+ ratio similar to the the neutral gas at $v \approx 0$ km/s. Finally, we note large corrections for Al^+, Si^+, and S^+ at $\log f_N(Fe^+) > -0.07$ which corresponds to a very large ionization parameter for the ionized component. At very high levels of ionization, the Si^+, S^+, and Al^+ ions exhibit significantly greater abundances relative to Fe^+. We doubt, however, that the gas considered here has $\log f_N(Fe^+) > -0.07$. As noted above, if the absorption at $v \approx -65$ km/s is representative of the ionization component in our two-phase model, then $\log f_N(Fe^+) < -0.1$. Furthermore, it is very unlikely (if not nonphysical) to assume that the neutral component contributes no Fe^{++} gas. Allowing some ionization of Fe^+ to Fe^{++} in the neutral component drives the effective $f_N(Fe^+)$ value even lower.

We have also performed a two-phase analysis assuming a series of Kurucz stellar spectra. Figure 9 presents the results assuming $N(\mathrm{HI}) = 10^{19}\,\mathrm{cm}^{-2}$, $T = 40000$ K, [Fe/H] $= -1$, and $Fe^{++}/Fe^+ = -0.5$ dex. The results are qualitatively similar to those from the Haardt-Madau spectra (Figure 8): Si^+, Al^+, S^+, Cr^+, and Ni^+ all require small negative ionization corrections relative to Fe^+ while N^0 and Ar^0 require large positive corrections. In contrast with the Haardt-Madau results, all of the corrections converge to 0 dex as $f_N(Fe^+) \to 1$. For a stellar atmosphere with $T = 40000$ K, one predicts significantly larger Fe^{++}/Fe^+ ratios than the Haardt-Madau spectrum, primarily due to the softer spectral slope of the stellar flux. In fact, adopting a higher effective temperature (e.g. 50000 K) for the stellar atmosphere brings the results into better qualitative agreement with the Haardt-Madau models. Finally, we have also considered different values of N(HI) in the ionized component than $10^{19}\,\mathrm{cm}^{-2}$. In general, lower N(HI) values lead to slightly larger $[X_i/Fe^+]$ values and higher N(HI) values imply smaller corrections. The differences are typically smaller than 0.1 dex, however, and are therefore on the level of the uncertainties inherent to our photoionization modeling.

To summarize, the two-phase scenario implies small but important corrections to the low-ion ratios. We favor this model over the single phase model because of the likelihood that the intermediate and low-ion components at $v \approx -26$ km/s are not exactly aligned. Furthermore, we have identified ionized gas near the damped Lyα system (at $v \approx -65$ km/s) which exhibit properties consistent with the ionized component of our two-phase model. Interestingly, the ionization corrections of the two-phase scenario lead to relative abundances which are less conflicting with the $v \approx 0$ km/s gas. The challenge of the two phase scenario in comparison with the single phase model, however, is that it introduces an additional gas component with another set of uncertainties related to HI column density, metallicity, geometry, etc. These uncertainties prohibit one from determining the $f_N(Fe^+)$ value and thereby precise ionization corrections.

5. DISCUSSION

In the previous sections, we carefully considered the ionization state of the gas comprising the damped Lyα system at $z = 2.62$ toward GB1759+7539. Qualitatively, we demonstrated that the gas in one major velocity component is primarily neutral ($x < 0.1$) while the remaining gas is partially ionized ($x \approx 0.5$). In both cases, significant ionization corrections for Ar^0 are required. Furthermore, several elements in the ionized component – notably N, S – require small but important ionization corrections to infer accurate elemental abundances from the low-ion column densities. These corrections have important implications for our measurements of the metallicity of this damped system and our interpretations of the nucleosynthetic enrichment and dust depletion inferred from relative chemical abundances. Before proceeding, we wish to emphasize that *this system exhibits a number of characteristics (e.g. variations among the low-ion profiles) which* *separate it from the majority of damped systems.* Therefore, one must be careful not to generalize the ionization properties of this system to the entire sample of damped systems. At the same time, it is worth noting that the H I column density of this system is significantly greater than the damped Lyα threshold of $2 \times 10^{20}\,\mathrm{cm}^{-2}$ and would not have been expected to be partially ionized on the basis of its H I optical depth.

TABLE 7
METALLICITY TABLE

Model	[Fe/H]	[Si/H]	[S /H]
HM: No IC	−1.26	−0.80	−0.81
HM: One-Phase	−1.31	−0.90	−0.71
HM: Two-Phase, $f(\mathrm{Fe^+})$=-0.1	−1.31	−0.95	−0.88
HM: Two-Phase, $f(\mathrm{Fe^+})$=-0.5	−1.39	−0.97	−0.91
KZ: One-Phase	−1.35	−0.92	−0.91
KZ: Two-Phase, $f(\mathrm{Fe^+})$=-0.1	−1.31	−0.95	−0.88
KZ: Two-Phase, $f(\mathrm{Fe^+})$=-0.5	−1.36	−0.97	−0.90

These metallicity values are for the entire damped Lya system. The photoionization corrections, however, have only been applied to the gas at $v \approx -26$ km/s and -47 km/s.

Consider first the impact of photoionization on the metallicity measurements of this damped Lyα system. We focus on the metallicity of the neutral hydrogen gas because estimating the metallicity of all hydrogen gas (ionized + neutral) would require assumptions on the distribution of HI as a function of velocity. In addition, the metallicity of the neutral component is more readily compared against theoretical models. In Table 7, we report a series of metallicity measurements for S, Si, and Fe assuming a variety of photoionization scenarios for the partially ionized gas[8]: (i) no corrections; (ii) a single-phase cloud with the HM spectrum; (iii,iv) a two-phase scenario using the HM spectrum with two different assumptions on the level of ionization in the ionized component; (v-vii) single and two-phase scenarios adopting the Kurucz spectrum with $T = 40000$ K. In the two-phase scenarios, the results are modestly sensitive to the N(HI) value assumed for the ionized component. For this discussion, we assume $N(\mathrm{HI}) = 10^{19}\,\mathrm{cm}^{-2}$.

The results presented in Table 7 indicate systematic offsets in the metallicity of this damped system when one adopts ionization corrections. In general, however, the photoionization corrections imply a small, statistically insignificant decrease in the [X/H] values. The $\lesssim 0.1$ dex corrections are on the same order as the 0.1 dex uncertainty in the N(HI) value. Therefore, even in the unlikely event that all of the damped Lyα systems require ionization corrections which are this large, it will have a relatively minor impact on the chemical evolution history currently resolved by the damped Lyα systems (e.g. Prochaska & Wolfe 2000). The one possible exception, however, is the chemical enrichment history derived from $\mathrm{Zn^+}$ whose photoionization balance is very poorly determined (Howk & Sembach 1999).

[8] Note that the effects of photoionization on the metallicity of this system are tempered by the fact that only ≈ 50% of the gas requires ionization corrections.

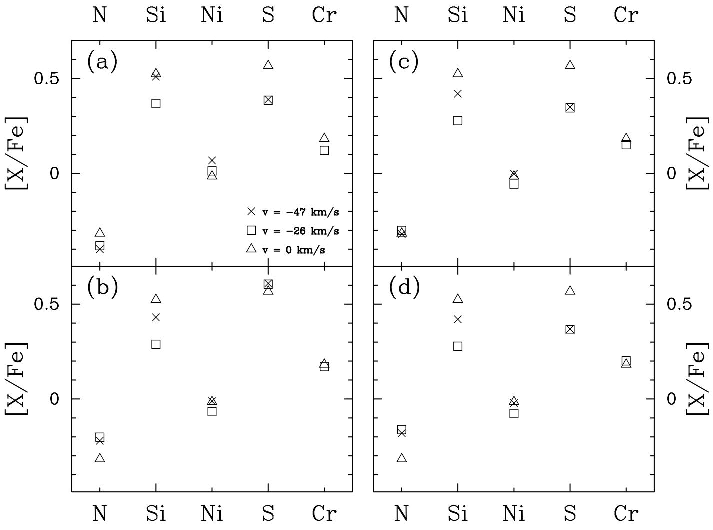

FIG. 10.— The relative abundance [X/Fe] of the three main velocity components in this damped system for the Haardt-Madau input spectrum. We consider (a) no ionization corrections; (b) a single-phase scenario; (c) a two-phase scenario with $f_N(\mathrm{Fe^+}) = -0.3$; and (d) a two-phase scenario with $f_N(\mathrm{Fe^+}) = -0.1$ dex. The ×'s mark the $v \approx -47$ km/s component, the Δ's mark the $v \approx -26$ km/s component, and the □'s mark the $v \approx 0$ km/s component.

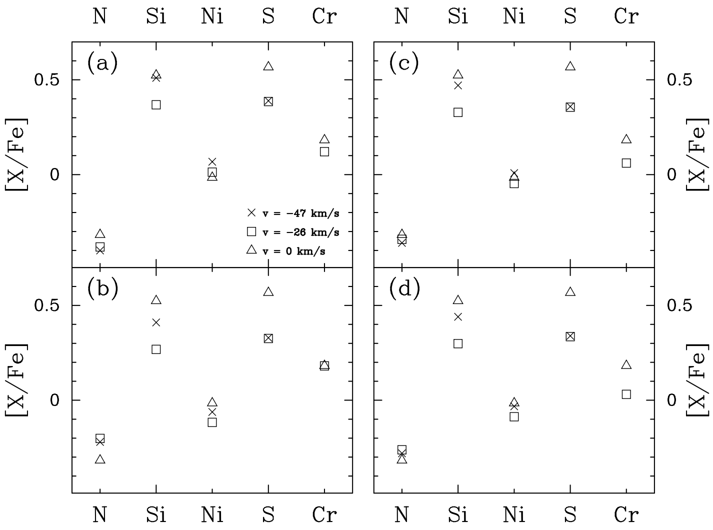

FIG. 11.— Same as Figure 10 but with the Kurucz input spectrum.

In contrast to the metallicity measurements where factors of 0.1 to 0.2 dex are generally unimportant, photoionization corrections can significantly influence our interpretations of the relative elemental abundances of the damped Lyα systems. A correction to $\mathrm{Si^+/Fe^+}$of 0.2 dex, for example, would imply a very different dust-to-gas ratio and/or nucleosynthetic enrichment history (e.g. Prochaska & Wolfe 2002). This point is well illustrated in Figures 10 and 11 which present the relative abundance [X/Fe] of the three main velocity components in this damped system for the Haardt-Madau and Kurucz input spectrum respectively. In each figure we consider (a) no ionization corrections; (b) a single-phase scenario; (c) a two-phase scenario with $f_N(\mathrm{Fe^+}) = -0.3$; and (d) a two-phase scenario with $f_N(\mathrm{Fe^+}) = -0.1$ dex.

Examining Figures 10 and 11 we find that the ratios of S/Fe and Si/Fe vary by > 0.1 dex among the various ionization models. Therefore, it is very difficult to assess the elemental abundances ratios of the *ionized gas* in this damped Lyα system. We are concerned that any damped system which is ionized to a similar degree will prove just as challenging. These uncertainties aside, we believe this system exhibits variations in its relative abundances independent of photoionization. These may be due to differential depletion and/or varying nucleosynthetic enrichment patterns. In either case, this is one of the few examples of a damped Lyα system where the abundances ratios are not uniform within statistical error.

The results of this paper highlight the importance of examining photoionization diagnostics in a larger sample of damped Lyα systems. Although $\mathrm{Al^{++}/Si^+}$ may provide a rough assessment of ionization (Vladilo et al. 2001), a more precise analysis can be performed if one acquires observations of adjacent ions like $\mathrm{Fe^+}$, $\mathrm{Fe^{++}}$ and $\mathrm{N^0}$, $\mathrm{N^+}$. Of course, the intermediate-ions require observations with coverage deep within the Lyα forest. While it may be important to consider a full photoionization analysis of the kind presented here for each damped Lyα system, we believe the following photoionization diagnostics (summarized in Table 8) can provide a 'first-look' analysis of the ionization state. In all cases, our conclusions are derived from the extensive set of CLOUDY photoionization models that we have described throughout the paper.

- The $\mathrm{Ar^0/(Si^+, S^+)}$ ratio is an excellent diagnostic for identifying systems with low ionization factors, $x \approx 0$. Specifically, a generic feature of photoionization models is that an observed value of $[\mathrm{Ar^0/(Si^+, S^+)}] > -0.2$ dex requires $x < 0.1$. For the 7 systems with Ar/Si measurements or limits (Molaro et al. 2001; Prochaska & Wolfe 2002), they all suggest $x < 0.1$ except GB1759+7539. It is also important to emphasize that a low $\mathrm{Ar^0/(Si^+,S^+)}$ ratio does not require $x \gg 0$ given its large reionization cross-section (Sofia & Jenkins 1998). In fact, we have argued that the gas at $v \approx 0$ km/s in the GB1759+7539 damped system has $x < 0.1$ even though it exhibits a significantly sub-solar $\mathrm{Ar^0/Si^+}$ ratio. Therefore, this diagnostic is only valuable for ruling out photoionization effects in a given damped system. Finally, we should note that the $\mathrm{Ar^0/(Si^+,S^+)}$ ratio could be affected by nucleosynthesis and/or dust depletion. On the other hand, Ar/S is solar in systems with a wide range of metallicity in the local universe (Henry & Worthey 1999) and the majority of damped systems exhibit [S/Si] ≈ 0 indicating differential depletion will not modify the Ar, S, or Si abundances.

- Unlike the $\mathrm{Ar^0/(Si^+, S^+)}$ ratio, a determination of the $\mathrm{Fe^{++}/Fe^+}$ ratio can establish whether a given damped system is predominantly neutral *or* ionized. We find $x < 0.1$ in systems where $\mathrm{Fe^{++}/Fe^+} < -1.6$ dex, and similarly, a system with $\mathrm{Fe^{++}/Fe^+} > -1$ dex will have $x > 0.5$. A further advantage of this diagnostic is that the $\mathrm{Fe^{++}/Fe^+}$ ratio is independent of nucleosynthesis or dust depletion. In short, an accurate measurement of $\mathrm{Fe^{++}}$ via the Fe III 1122 transition is an extremely valuable probe of the ionization state of any quasar absorption line system.

- The $\mathrm{N^+/N^0}$ ratio places similar constraints on x as the $\mathrm{Fe^{++}/Fe^+}$ diagnostic. We find $x < 0.1$ in systems showing $\mathrm{N^+/N^0} < -1$ dex and $x > 0.5$ in systems where $\mathrm{N^+/N^0} > -0.2$ dex.

Table 8
PHOTOIONIZATION DIAGNOSTICS

Ratio	$x < 0.1$	$x > 0.5$	Comment
$\mathrm{Ar^0/(Si^+,S^+)}$	> -0.2	N/A	Sensitive to dust, nucleo
$\mathrm{Fe^{++}/Fe^+}$	< -1.6	> -1	Lyα forest
$\mathrm{N^+/N^0}$	< -1	> -0.2	Lyα forest

In passing, we wish to comment on the implications of photoionization for our kinematic modeling of the damped Lyα systems (e.g. Prochaska & Wolfe 1997). To assess the kinematic characteristics of an individual damped Lyα system we choose a single, high S/N low-ion profile as representative of the neutral gas for the entire system. This approach was motivated by the fact that the low-ion profiles track one another very closely (e.g. Prochaska & Wolfe 1996). In the case of the damped Lyα system studied here, we have found significant variations from low-ion to low-ion even prior to photoionization corrections. This variation will have a very small impact on the measured velocity width (Δv; c.f. Prochaska & Wolfe 1997) of the damped Lyα system, but the variations could impact the various shape parameters implemented in our analysis. Although this causes us some concern, we emphasize that this system is unusual for exhibiting a significant variation among the low-ion profiles. In a future paper, we will demonstrate the excellent chemical and ionization uniformity observed in the large majority of damped Lyα systems (Prochaska et al. 2002).

We also wish to reflect on the impact of photoionization regarding the relationship between the observed C II* profile and star formation (see Wolfe et al. 2002 for a more complete discussion). As noted in the introduction, the C II* profile of the GB1759+75 damped system does not closely track the other low-ion profiles (Figure 1). Specifically, the C II* profile exhibits much greater optical depth at $v \approx 0$ km/s than $v \approx -26$ km/s. We believe the gas at $v \approx 0$ km/s has properties similar to the Cold Neutral Medium of the Galactic ISM (e.g. Savage and Sembach 1996). In contrast, if the gas at $v \approx -26$ km/s has physical properties similar to the Warm Neutral Medium or Warm Ionized Medium of the Galactic ISM, then we would predict a low C II* optical depth relative to the other low-ions, as observed. Therefore, we believe the components at $v \approx 0$ and -26 km/s represent two distinct phases of gas. The net effect is that it is difficult to assess the star formation rate within this damped Lyα system from its measured C II* column density.

Finally, we wish to outline other avenues for investigating the ionization state of the damped Lyα systems. One might gain important insight into the properties of ionized gas associated with damped systems by performing a comprehensive analysis of the quasar absorption line systems with N(HI) $\approx 10^{19.5}$cm^{-2} (e.g. Prochaska & Wolfe 1999; O'Meara et al. 2001). These 'sub-DLAs' may show a wide range of ionization states and would provide an excellent test of the modeling implemented throughout this paper. Furthermore, they are far more numerous than the damped systems and one may design specific observational experiments to focus on their ionization states (e.g. preselect systems where Si^{++}, N^{+} etc. readily observed). Another more efficient approach would be to examine lower redshift systems where the Lyα forest is a far less compromising effect. The challenge here remains identifying enough systems toward very bright quasars; a challenge which will be alleviated in part with the introduction of COS on the Hubble Space Telescope.

The authors wish to extend special thanks to those of Hawaiian ancestry on whose sacred mountain we are privileged to be guests. Without their generous hospitality, none of the observations presented herein would have been possible. We wish to thank R. Carswell, F. Chaffee, and P. Outram for sharing their spectrum of GB1759+75. We acknowledge the very helpful Keck support staff for their efforts in performing these observations. Finally, we thank Gary Ferland and CLOUDY associates for the CLOUDY software package. This work was partially supported by NASA through a Hubble Fellowship grant HF-01142.01-A awarded by STScI to JXP. JCH acknowledges support from NASA grant NAG5-10957 and from NASA Long Term Space Astrophysics grant NAG5-3485 through the Johns Hopkins University. The work of DT, NS, JMO, and DK was funded in part by grant NASA funds G-NASA/NAG5-3237 and NAG5-9224, and by NSF grant AST-9900842. AMW was partially supported by NSF grant AST 0071257.

REFERENCES

Bergeson, S.D. & Lawler, J.E. 1993, ApJ, 408, 382
Bergeson, S.D. & Lawler, J.E. 1993b, ApJ, 414, L137
Bergeson, S.D., Mullman, K.L., Wickliffe, M.W., Lawler, J.E., Litzen, U., and Johansson, S. 1996, ApJ464, 1044
Bergeson, S.D., Mullman, K.L., & Lawler, J.E., 1996, ApJ464, 1050
Fan, X.-M. & Tytler, D. 1994, ApJS, 94, 17
Fedchak, J. A. & Lawler, J. E. 1999, ApJ, 523, 734
Fedchak, J. A., Wiese, L. M., & Lawler, J. E. 2000, ApJ, 538, 773
Ferland, G. J. 2001, PASP, 113, 41
Haardt, F. & Madau, P. 1996, ApJ, 461, 20
Henry, R.B.C. & Worthey, G. 1999, PASP, 111, 919
Howk, J.C. & Sembach, K.R. 1999, ApJ, 523, L141
Howk, J.C., Sembach, K.R., Roth, K.C., & Kruk, J.W. 2000, ApJ, 544, 867
Izotov, Y.I., Schaerer, D., & Charbonnel, C. 2001, ApJ, 549, 878
Kurucz, R.L. 1988, Trans. IAU, XXB, ed. M. McNally, (Dordrecht: Kluwer), p. 168-172
Lu, L., Sargent, W.L.W., Barlow, T.A., Churchill, C.W., & Vogt, S. 1996, ApJS, 107, 475
Molaro, P., Bonifacio, P., Centurión, M., D'Odorico, S., Vladilo, G., Santin, P., & Di Marcantonio, P. 2000, ApJ, 541, 54
Molaro, P., Levshakov, S.A., D'Odorico, S., Bonifacio, P., & Centuríon, M. 2001, ApJ, 549, 90
Morton, D.C. 1991, ApJS, 77, 119
Morton, D.C. 2002, in preparation
O'Meara, J.M., Tytler, D., Kirkman, D., Nao, S., Prochaska, J.X., Lubin, D., & Wolfe, A.M. 2001, ApJ, 522, 718
Outram, P.J., Chaffee, F.H., & Carswell, R.F. 1999, MNRAS, 310, 289
Pettini, M., Smith, L. J., Hunstead, R. W., and King, D. L. 1994, ApJ, 426, 79
Pettini, M., Ellison, S.L., Steidel, C.C., & Bowen, D.V. 1999, ApJ, 510, 576
Prochaska, J. X. & Wolfe, A. M. 1996, ApJ, 470, 403
Prochaska, J. X. & Wolfe, A. M. 1997, ApJ, 486, 73
Prochaska, J. X. & Wolfe, A. M. 1999, ApJS, 121, 369
Prochaska, J.X. & Wolfe, A.M., 2000, ApJ, 533, L5
Prochaska, J.X., Wolfe, A.M., Tytler, D., Burles, S.M., Cooke, J., Gawiser, E., Kirkman, D., O'Meara, J.M., & Storrie-Lombardi, L. 2001, ApJS, 137, 21
Prochaska, J.X. & Wolfe, A.M., 2002, ApJ, in press
Prochaska, J.X. et al. 2002, in preparation
Savage, B. D. and Sembach, K. R. 1996, ARA&A, 34, 279
Schectman, R.M., Povolny, H.S., & Curtis, L.J. 1998, ApJ, 504, 921
Sembach, K.R., Howk, J.C., Ryans, R.S.I., & Keenan, F.P. 2000, ApJ, 528, 310
Shapiro, P.R., & Moore, R.T. 1976, ApJ, 207, 460
Sofia, U.J. & Jenkins, E.B. 1998, ApJ, 499, 951
Shull, J.M., & Slavin, J.D. 1994, ApJ, 427, 784
Sutherland, R.S. & Dopita, M.A. 1993, ApJS, 88, 253
Viegas, S.M. 1995, MNRAS, 276, 268
Vladilo, G., Centurión, M., Bonifacio, P., & Howk, J.C. 2001, ApJ, 557, 1007
Vogt, S.S., Allen, S.L., Bigelow, B.C., Bresee, L., Brown, B., et al. 1994, SPIE, 2198, 362
Webb, J.K., Murphy, M.T., Flambaum, V.V., Dzuba, V.A., Barrow, J.D., Churchill, C.W., Prochaska, J.X., & Wolfe, A.M. 2001 Phys. Rev. Lett. 87, in press
Wolfe, A. M. & Prochaska, J.X. 2000, ApJ, 545, 591
Wolfe, A. M., Prochaska, J.X., & Gawiser, E. 2002, in preparation